Primary cilia drive postnatal tidemark patterning in articular cartilage by coordinating responses to Indian Hedgehog and mechanical load

Danielle Rux[1]*, Kimberly Helbig[1], Biao Han[2], Courtney Cortese[1], Eiki Koyama[1], Lin Han[2], Maurizio Pacifici[1]

[1]Translational Research Program in Pediatric Orthopaedics, Children's Hospital of Philadelphia

[2]Drexel University, Philadelphia, PA

Correspondence to:

Danielle Rux

The Children's Hospital of Philadelphia

Division of Orthopaedic Surgery

Translational Research Program in Pediatric Orthopaedics

Abramson Research Center, Suite 902

3615 Civic Center Blvd.

Philadelphia, PA 19104

ruxd@chop.edu

Running Title: Primary cilia are required for articular cartilage tidemark patterning

Keywords: Primary cilia, IFT88, Gdf5, Synovial joint development, Hedghog, Tidemark, Prg4

Competing Interests: None declared

ABSTRACT

Articular cartilage (AC) is essential for body movement, but is highly susceptible to degenerative diseases and has poor self-repair capacity. To improve current subpar regenerative treatment, developmental mechanisms of AC should be clarified and, specifically, how postnatal multi-zone organization is acquired. Primary cilia are cell surface organelles crucial for mammalian tissue morphogenesis and while the importance of chondrocyte primary cilia is well appreciated their specific roles in postnatal AC morphogenesis remain unclear. To explore these mechanisms, we used a murine conditional loss-of-function approach (*Ift88-flox*) targeting joint-lineage progenitors (*Gdf5Cre*) and monitored postnatal knee AC development. Joint formation and growth up to juvenile stages were largely unaffected, however mature AC (aged 2 months) exhibited disorganized extracellular matrix, decreased aggrecan and collagen II due to reduced gene expression (not increased catabolism), and marked reduction of AC modulus by 30-50%. In addition, we discovered the surprising findings that tidemark patterning was severely disrupted and accompanied alterations in hedgehog signaling that were also dependent on regional load-bearing functions of AC. Interestingly, *Prg4* expression was also increased in those loaded sites. Together, our data provide evidence that primary cilia orchestrate postnatal AC morphogenesis, dictating tidemark topography, zonal matrix composition and mechanical load responses.

42 **INTRODUCTION**

43 Body movement requires uniquely shaped synovial joints to maximize range and type of
44 motion based on anatomical location and load-bearing needs (Mow & Sugalski, 2001). Much has
45 been learned about the structure and function of adult joint tissues –articular cartilage (AC),
46 meniscus and intra joint ligaments– including the biomechanical and lubricating roles each tissue
47 plays in sustaining motion and resilience (Longobardi et al., 2015). While it is clear that the
48 majority of morphogenesis and terminal organization of mature AC occurs during postnatal life
49 in coordination with growth of the skeleton (Decker, 2017; Decker et al., 2017; Kozhemyakina et
50 al., 2015; L. Li et al., 2017), cellular mechanisms remain poorly understood. A full
51 understanding of this morphogenetic process would be critical to inform on how joint
52 developmental defects/diseases are established and, as importantly, how defective and damaged
53 joint tissues could be repaired and regenerated.

54 In adults, fully mature AC displays a stereotypic zonal organization of cells and
55 extracellular matrix (ECM) that contains both non-mineralized and mineralized layers. The non-
56 mineralized hyaline cartilage includes: (i) a top superficial zone of flat cells juxtaposed with the
57 synovial space and parallel to the surface, producing ECM components such as lubricin/*Prg4*;
58 (ii) an intermediate zone of round chondrocytes amidst aggrecan and randomly aligned collagen
59 II fibrils; (iii) a thick, deep zone of polarized chondrocytes oriented into columns and containing
60 abundant ECM rich in aggrecan and with collagen II fibrils aligned perpendicular to the surface.
61 The mineralized cartilage comprises a bottom zone with large hypertrophic-like chondrocytes
62 that conjoins AC to the underlying subchondral bone (Hunziker et al., 2007). The tidemark
63 represents the mineralization front demarcating the boundary between non-mineralized and
64 mineralized cartilage. While, little is known of is developmental origins, significant evidence

65 exists that the tidemark advances toward the cartilage surface with age (Johnson, 1962; Lane &
66 Bullough, 1980; Loeser et al., 2012; Oegema et al., 1997; Radin et al., 1991) or with alterations
67 in mechanical load (Nomura et al., 2017; O'Connor, 1997; Tomiya et al., 2009), reducing non-
68 mineralized cartilage thickness. In addition, the transitioning of aquatic axolotl salamanders to
69 terrestrial life results in the formation of a tidemark (Cosden-Decker et al., 2012; Rux et al.,
70 2019), suggesting ambulation influences initial positioning. Despite these observations, no
71 cellular mechanisms on tidemark patterning or disease-state repositioning have been clarified.
72 Postnatal AC morphogenesis is complex as it needs to eventually establish a highly
73 structured, anisotropic tissue critical for joint mechanical function (Gannon et al., 2015;
74 Hunziker et al., 2007; Julkunen et al., 2009). Recent studies by our group and others have led to
75 a better understanding of the basic tenets of postnatal morphogenesis of AC in mouse knee joints
76 (Decker et al., 2017; Kozhemyakina et al., 2015; L. Li et al., 2017). At birth, nascent AC is
77 disorganized and contains a pool of highly proliferative progenitors which give rise to all of the
78 cells in adult AC. By 2-3 weeks of age, AC is matrix-rich, but still lacks a clear zonal
79 organization. By 8 weeks, the stereotypical zonal organization is established. Importantly, we
80 found that cell proliferation decreases rapidly soon after birth while the tissue continues to
81 thicken through matrix production/accumulation and increases in average cell size (Decker et al.,
82 2017). Thus, there are three stages to postnatal AC development: proliferation (neonatal), growth
83 (adolescent) and maturation (adult). Lineage tracing in our recent study strongly suggested that
84 chondrocytes establish zonal organization and vertical columns during the maturation phase
85 (Decker et al., 2017), but the mechanisms by which this could occur have not been elucidated.
86 Primary cilia are putative mechano- and morphogen-transducing cell surface organelles
87 present on nearly every cell in mammals and are crucial for tissue morphogenesis. Cytoskeletal

88 regulation, cell polarity and a number of signaling pathways (e.g., hedgehog, wnt and TGFβ) are
89 governed, at least in part, by the primary cilium (Goetz & Anderson, 2010; Wheway et al.,
90 2018). The chondrocyte primary cilium is an important regulator of cartilage function (Haycraft
91 et al., 2007; Serra, 2008; Yuan & Yang, 2016) and lengthening has been correlated with human
92 osteoarthritis (OA) (McGlashan et al., 2008). In mice, conditional loss of function in AC results
93 in deficits that often lead to early onset osteoarthritis (OA) (Chang et al., 2012; Irianto et al.,
94 2014; Sheffield et al., 2018; Song et al., 2007; Yuan & Yang, 2015). It is thus clear that primary
95 cilia are important to AC health, but the specific mechanisms by which they function during
96 postnatal morphogenesis remain unclearly defined.

97 In an effort to identify mechanisms of postnatal AC development in mice and how cilia
98 function in this regard, we developed a joint-specific (*Gdf5Cre*) disruption of primary cilia
99 (*IFT88-flox*) and delineated AC development up to 8 weeks of age. We found that while the
100 disruption of primary cilia does not affect embryonic or early postnatal growth through 3 weeks
101 of age, it significantly altered AC maturation including ECM production and organization,
102 culminating in reduced AC modulus at 8 weeks of age. Surprisingly, we also found significant
103 disruptions in tidemark patterning that altered the organization of mineralized and non-
104 mineralized zones. Our mechanistic studies revealed primary deficits in hedgehog signaling
105 starting at 3 weeks accompanied by secondary changes to BMP and TGFβ signaling by 8 weeks.
106 Importantly, our data indicate that the hedgehog pathway drives tidemark patterning and location
107 during postnatal AC morphogenesis, being the first to identify a signaling mechanism that is
108 capable of regulating and altering the tidemark.
109
110

111 **RESULTS**

112 ***Gdf5Cre* is joint specific and conditional deletion of *IFT88* results in loss of primary cilia.**

113 In order to target primary cilia specifically in synovial joints, we used *Gdf5Cre* in
114 combination with an *IFT88* conditional allele. *Gdf5* is a unique marker for the embryonic
115 mesenchymal progenitor cells of synovial joints called the interzone. *Gdf5Cre* faithfully marks
116 these cells in the embryo and lineage-traces to all of the mature tissues of synovial joints (Decker
117 et al., 2017; Koyama et al., 2008) (Fig. 1Aa-c) but not growth plate chondrocytes (Fig. 1Ad). In
118 order to study primary cilia, we combined *Gdf5Cre* with an *IFT88* conditional allele whose
119 product (Intraflagellar Transport Protein 88) is important in anterograde transport in cilia and
120 maintenance of the cilium structure. The result is loss of primary cilia in *Gdf5*-expressing
121 interzone cells and in adult synovial joints. We visualized primary cilia using an antibody against
122 acetylated tubulin and found they were present on nearly every chondrocyte in control AC (Fig.
123 1Ba-b) and in the growth plate (Fig. 1Bc and Bf) but a significant loss in all zones of AC in
124 mutant animals (Fig. 1Bd-e) confirming our model was reliable.

125

126 **Joint-specific deletion of *IFT88* leads to disrupted AC tidemark patterning and inferior**
127 **biomechanical function.**

128 Next, we evaluated histology and performed mechanical testing to assess the
129 consequences of loss of primary cilia during postnatal AC morphogenesis. We used safranin O
130 staining to visualize basic histology and proteoglycans in the ECM (Fig. 2A). At birth, nascent
131 AC of mutants was indistinguishable from controls (Fig. 2Aa-b, brackets). Up to 3 weeks,
132 immature AC developed similarly (Fig. 2Ac-d) and higher magnification images revealed no
133 discernible differences in cell morphology or patterning (Fig. 2Ae-h). However, at 8 weeks we

134 noted irregular accumulation of the interterritorial ECM (arrows) and chondrocyte size
135 (asterisks) in the femoral condyle (Fig. 2Ai-l) and a consistent reduction of safranin O in the
136 tibial plateau (Fig. 2i-j, m-n). Thus, the loss of IFT88 primarily affected the maturation phase of
137 postnatal AC morphogenesis. Growth plates were unaffected at all stages consistent with no
138 recombination from *Gdf5Cre* (Fig. S1). Next, we utilized a combination of safranin O-stained
139 sections and sections imaged with Differential Interference Contrast (DIC) to quantify AC
140 thickness, AC composition of mineralized and non-mineralized cartilage and also cell density.
141 These analyses revealed several notable changes. First, in healthy AC, the tidemark (Fig. 2B,
142 dashed yellow line) closely followed the contour of the femoral condyle surface 2-3 cell layers
143 below, but was relatively flat in the load-bearing region of the tibial plateau located about 5-6
144 cell layers from the surface (Fig. 2Ba, bracket). In mutants, the tidemark was often difficult to
145 visualize, but followed an irregular path in the femoral condyle and was flat, but noticeably
146 further from the surface in the tibial plateau (Fig. 2Bb, bracket). Quantifying AC composition as
147 a percent area, we found that non-mineralized cartilage constituted approximately 31% of the
148 femoral condyle and 51% of tibial plateau AC in control animals; this increased slightly in
149 mutant femoral condyle AC to 36% and significantly in tibial plateau AC to 70% (Fig. 2C). For
150 consistency, we measured AC height at its thickest regions in each tissue section. We found no
151 changes in AC thickness at 3 weeks nor in tibial plateau AC at 8 weeks, but the AC height was
152 significantly higher in the thickest regions of mutant femoral condyles (Fig. 2Da-b). Bisected
153 into mineralized and non-mineralized cartilage at 8 weeks, we found similar trends in
154 composition from Fig. 2C. In the femoral condyle, mutants showed a significant increase in non-
155 mineralized thickness, but no change mineralized thickness (Fig. 2Dc) and in the tibial plateau,
156 mutants showed a significant increase in non-mineralized cartilage and decrease in mineralized

157 cartilage (Fig. 2Dd). Thus, AC composition in tibial plateau is consistently more non-
158 mineralized whereas mineralization is much more variable in the femoral condyle but follows the
159 same trend. Interestingly, we found that cell density in non-mineralized AC was significantly
160 reduced in both regions of mutant AC (Fig. 2E).

161 To assess possible functional consequences of these morphologic changes in mature AC,
162 we used atomic force microscopy (AFM)-nanoindentation to measure AC stiffness. We
163 measured two regions on the medial tibial plateau (the edge covered by meniscus and the center
164 load-bearing region) and one region on the femoral condyle. In all regions of interest, the
165 indentation modulus (i.e. resistance to deformation) was significantly decreased in mutants (Fig.
166 2F). Thus, loss of IFT88 in AC results in impaired load-bearing function during tissue
167 maturation.

168

169 **IFT88 regulates chondrocyte fate and matrix deposition in mineralized and non-**
170 **mineralized zones.**

171 Next, we performed immunofluorescence staining for several key ECM and chondrocyte-
172 specific markers. Collagen II is a major structural component of cartilage ECM, responsible for
173 tensile strength of the tissue (Mow & Ratcliffe, 1997). In control animals, it was uniformly
174 dispersed in AC at 3 weeks and 8 weeks (Fig. 3Aa and Ac). In mutant animals, we noted no
175 changes at 3 weeks (Fig. 3Ab) and a mild reduction at 8 weeks (Fig. 3Ad). Collagen X is a
176 marker of hypertrophic and mineralizing chondrocytes. We found collagen X similarly localized
177 to cells juxtaposed to the developing secondary ossification center in control (Fig, 3Ba, c) and in
178 mutant AC (Fig. 3Bb, d) consistent with a lack of precocious hypertrophy closer to the AC
179 surface. Aggrecan is the major proteoglycan in cartilage ECM that gives it its compressive load-

180 bearing and energy dissipation properties. In healthy tissue, it was uniformly deposited in the
181 entire thickness of developing AC at 3 weeks (Fig. 3Ca) and was enriched in non-mineralized
182 cartilage at 8 weeks (Fig. 3Cc). A clear boundary (i.e., tidemark) could be visualized where the
183 aggrecan-low mineralized cartilage met the aggrecan-rich non-mineralized cartilage (Fig. 3Cc,
184 arrows). In IFT88 mutants, aggrecan deposition was comparable to controls in immature
185 cartilage at 3 weeks (Fig. 3Cb), but notable disorganization, lack of tidemark and variable
186 deposition (high, arrows and low, arrowheads) were all apparent in mature cartilage at 8 weeks
187 (Fig. 3Cd). Sox9 is considered a master transcriptional regulator of chondrocyte fate and can
188 directly regulate the expression of aggrecan and collagen II (Lefebvre et al., 2019). In immature
189 AC, Sox9 was present uniformly in articular chondrocytes of controls and mutants at 3 weeks
190 (Fig. 3Da-b) consistent with the uniform distribution of collagen II and aggrecan at this stage. In
191 mature AC, Sox9-positive cells were largely restricted to the non-mineralized cartilage (Fig.
192 3Dc), as visualized by DIC imaging (Fig. S2a-c), and is consistent with a recent report of Sox9
193 function in AC (Haseeb et al., 2021). Mutant tissues at 8 weeks continued to express Sox9
194 broadly in non-mineralized chondrocytes (Fig. S2d-f), but Sox9-positive cells could also be seen
195 in articular chondrocytes beneath the tidemark in the femoral condyle (Fig. 3Dd, arrows). Taken
196 together, these data show that IFT88 mutants display an altered pattern of non-mineralized
197 chondrocytes and coordinately disrupted ECM in mature AC, but not immature AC.
198 Pericellular matrix (PCM) creates a thin microenvironment surrounding chondrocytes
199 within the broader ECM and is considered a crucial transducer of biomechanical signals (Guilak
200 et al., 2006). To observe any changes to the PCM, we performed immunofluorescence staining
201 for perlecan, a biomarker of cartilage PCM (Kvist et al., 2008; Wilusz et al., 2012). In immature
202 AC at 3 weeks, perlecan was broadly distributed in both control and mutant tissues (Fig. 3Ea-b).

203 In mature AC 8 weeks, perlecan was localized to chondrocytes nearest to the surface in control
204 tissue (Fig. 3Ec) and high magnification images overlaid with DIC imaging revealed restriction
205 to the non-mineralized cartilage above the tidemark (Fig. 3Ed-e, arrows). The organization of
206 perlecan deposition was significantly disrupted in mutant AC at 8 weeks (Fig. 3Ed). In the
207 femoral condyle, chondrocytes with perlecan-rich PCM could be visualized far below the
208 tidemark (Fig. 3Eg, asterisks), and in tibial plateau AC there was an expansion of perlecan-
209 positive chondrocytes in the load-bearing region above the tidemark (Fig. 3Eh). Together, these
210 data provided strong evidence that loss of IFT88 in AC disrupts tidemark patterning and
211 chondrocyte fate/microenvironment during postnatal maturation.
212
213 **Loss of IFT88 in AC does not increase matrix degradation.**
214 Previous *in vitro* studies have shown that primary cilia, and IFT proteins, regulate ECM
215 proteases in chondrocytes (Coveney et al., 2018). To test whether this applied to our *in vivo*
216 model, we performed immunofluorescence staining or *in situ* hybridization for MMP13
217 (collagenase), Adamts4 and Adamts5 (aggrecanases) at 8 weeks. MMP13 was unchanged in
218 mutants and was restricted to the base of AC at the transition to subchondral bone (Fig. 4A). We
219 used RNAscope (FastRed detection) to perform *in situ* hybridization and took advantage of
220 FastRed fluorescence for imaging low-expressing genes. In AC, we found no expression of
221 either *adamts4* or *adamts5* in control or mutant AC at 8 weeks (Fig. 4B-C). To ensure these data
222 were reliable, we compared to other tissues in and around the joint. *Adamts4* (Fig. S3A) was
223 expressed in primary spongiosa beneath the growth plate (PS, arrowheads) and in periosteum
224 (PO, arrows) and *Adamts5* (Fig. S3B) was highly expressed by inner synovial fibroblasts in both

225 controls and mutants. These data indicate that the changes observed in aggrecan and collagen II
226 deposition in mutant AC (Fig. 2) were not caused by matrix degradation.
227
228 **Altered ECM in mature mutant AC are the result of transcriptional changes.**
229 To assess transcriptional changes of *Col2a1*, *Acan* and *Prg4*, we utilized RNAscope
230 (fastRed detection) imaged these high-expressing genes with brightfield. At 3 weeks, C*ol2a1* and
231 *Acan* were broadly expressed in immature AC of both mutants and controls (Fig. 5. Aa-d)
232 consistent with our findings from immunofluorescent staining at this stage described above (Fig.
233 3A and C). *Prg4* (lubricin) is important for protecting AC from OA (Chavez et al., 2019; Coles
234 et al., 2010; Marcelino et al., 1999; Rhee et al., 2005; Ruan et al., 2013). At 3 weeks, *Prg4* was
235 highly expressed in cells near the surface in control animals (Fig. 5Ae) and we found a
236 significant reduction in mutant AC (Fig. 5Af). In mature AC of control animals, *Col2a1* (Fig.
237 5Ba-b) and *Acan* (Fig. 5Be-f) transcripts were localized to layers of AC corresponding with the
238 domain of non-mineralized cartilage 2-3 layers deep in the femoral condyle and 5-6 layers deep
239 in the tibial plateau (Fig. 2Ba). In mutant AC, both *Col2a1* and *Acan* expression appeared much
240 more disorganized particularly in the femoral condyle (Fig. 5Bc and Bg, arrows). Higher
241 magnification images of mutants (Fig. 5Bd and Bh) and controls (Fig. 5Bb and Bf), highlighted
242 the clear disorganization of gene expression in all mutant cartilage, consistent with dysregulated
243 tidemark patterning, ECM deposition and deviant Sox9-positive cells outside the non-
244 mineralized cartilage (Fig. 2 and 3). In addition, mutants displayed broadly reduced expression
245 per cell of *Col2a1* and *Acan* in the load-bearing region of the tibial plateau compared to this
246 region in controls. Lastly, we found that *Prg4* at 8 weeks was highly expressed and uniformly
247 distributed in cell layers closest to the AC surface (extending a bit deeper in the tibial plateau

248 than in the femoral condyle) (Fig. 5Bi-j, bracket). In mutants, *Prg4* in the femoral condyle
249 displayed a patchy but overall decreased expression profile (Fig. 5Bl-k, arrows) and in the tibial
250 plateau we found a striking increase in *Prg4* in the load-bearing region (Fig. 5Bl-k, asterisk and
251 bracket). These data suggest that reduction/disorganization of collagen II and aggrecan
252 deposition in mature cartilage were due to changes at the transcriptional level and that,
253 surprisingly, *Prg4* expression was altered in both immature and mature cartilage of mutants.
254
255 **Primary cilia impart load/location-dependent functions for key chondrogenic pathways.**
256 Primary cilia are considered a signaling nexus that have some regulatory function in most
257 major signaling pathways (Anvarian et al., 2019). TGFβ (transforming growth factor β) and
258 BMP (bone morphogenetic protein) regulate chondrocyte fate and ECM anabolism by distinct
259 mechanisms via downstream SMAD-dependent mechanisms (Thielen et al., 2019). While TGFβ
260 largely maintains non-mineralized chondrocyte function and prevents hypertrophy (Chen et al.,
261 2012; Ferguson et al., 2000; Ionescu et al., 2003; Kang et al., 2005; Kim et al., 2012; Leboy et
262 al., 2001; T.-F. Li et al., 2010; Seo & Serra, 2007; Yang et al., 2001), BMP can influence both
263 non-mineralized and mineralized functions dependent on context (Bae et al., 2007; Fujii et al.,
264 1999; Horiki et al., 2004; Javed et al., 2008, 2009; Phimphilai et al., 2006). To assess the
265 involvement of these pathways, we used immunofluorescence for pSmad2 (TGFβ) or pSmad159
266 (BMP). In immature AC at 3 weeks, pSmad2-positive cells were broadly distributed in all layers
267 (Fig. 6Aa) while pSmad159-positive cells were largely present in the deepest layers of cartilage
268 (Fig. 6Ba). These patterns were unchanged in mutant cartilage (Fig. 6Ab and Bb). In mature AC,
269 pSmad2 overlapped significantly with Sox9 in controls and mutants (Fig. 6C) indicating
270 restriction to non-mineralized cartilage. The percentage of pSmad2-positive cells in control and

271 mutant non-mineralized cartilage was unchanged but the density of pSmad2-positive cells
272 decreased significantly in mutant tibial plateau (Fig. 6D). We performed parallel experiments for
273 pSmad159 and found similar overlap with Sox9 in control AC and in the mutant femoral
274 condyle, but a significant loss in mutant tibial plateau (Fig. 6E). Quantification showed
275 significant reductions in the percent pSmad159-positive cells and also cell density in this region
276 (Fig. 6F). These data suggest that disruption of IFT88 leads to alterations in BMP and, to a lesser
277 degree, TGFβ signaling in the load-bearing region of the tibial plateau simultaneously with ECM
278 disruptions already described.

279 Hedgehog signaling is a major regulator of chondrocyte function and is dependent on the
280 primary cilium for proper transduction through processing of Gli transcriptional effectors for
281 pathway activation or repression (Wheway et al., 2018). In the absence of hedgehog ligands
282 (Sonic, Desert or Indian), the transmembrane receptor Patched1 (Ptch1) inhibits the
283 transmembrane protein Smoothened (Smo) to sequester Gli factors in the cytoplasm. When
284 Hedgehog ligand is present, it binds Ptch1, the inhibition on Smo is relieved and Gli proteins are
285 processed into active forms that translocate to the nucleus for transcriptional activation. Thus,
286 loss of primary cilia generally results in loss of hedgehog signaling.

287 We sought to elucidate a possible role for hedgehog signaling in our AC model. To
288 visualize active signaling, we used the *Gli1-LacZ* reporter mouse in combination with whole
289 mount staining and imaging. Background staining was monitored using *Gli1-LacZ* negative
290 tissues (Fig. S4). We noted several key findings. First, hedgehog signaling was highly active in
291 immature AC of control animals at 3 weeks (Fig. 7A-B), and tissue sections revealed differences
292 in *Gli1-LacZ* patterning of the femoral condyle and loaded region of the tibial plateau, localized
293 to the first 3-4 cells layers of the femoral condyle (Fig. 7Aa) and to the bottom 3-4 cells layers in

294 the tibial plateau (Fig. 7Bb). *Gli1-LacZ* persisted in mature AC at 8 weeks (Fig. 7E and F) with
295 similar cell layer patterning of immature cartilage (Fig. 7Ee and Ff). *Gli1-LacZ* of immature
296 mutant cartilage was strongly down-regulated in both the femoral condyle (Fig. 7C and Cc) and
297 the tibial plateau (Fig. 7D and Dd). In mature mutant femoral condyle AC, *Gli1-LacZ* repression
298 was maintained from 3 weeks (Fig. 7G and Gg) but AC in the load-bearing region of the tibial
299 plateau exhibited very strong *Gli1-LacZ* up-regulation (Fig. 7H) including the surface zone cells
300 that control animals did not display (Fig. 7Hh). Taken together, the data show significant
301 hedgehog signal disruption before a structural AC phenotype is apparent, largely consistent with
302 known roles for primary cilia in hedgehog signaling. However, our data also shows hyperactive
303 *Gli1-LacZ* activity in the absence of primary cilia but in the presence of high mechanical load
304 during ambulation suggesting load-dependent alterations.
305
306 **Hedgehog response patterning is coupled to tidemark patterning; both are disrupted in**
307 **IFT88 mutants.**
308 Hedgehog signaling during embryonic development is tightly linked to tissue patterning
309 through established gradients of ligand distribution. A notable example of this is neural tube
310 formation where cells establish specific identities dependent on their exposure, and response, to
311 hedgehog ligands (Ribes & Briscoe, 2009) and fine-tuned by a number of co-
312 activators/antagonists (Allen et al., 2007, 2011; Holtz et al., 2013). Zonal chondrocyte
313 patterning of the growth plate is also dependent on hedgehog exposure in a signaling loop that
314 requires *Indian Hedgehog* (*Ihh*)-expressing pre-hypertophic chondrocytes and *Parathyroid*
315 *related protein* (*Pthrp*)-expressing reserve zone chondrocytes (Kronenberg, 2006; St-Jacques et
316 al., 1999). Hedgehog signaling patterns have not been well established in AC.

317 Using RNAscope, we assessed two major hedgehog response genes (*Gli1* and *Ptch1*) as
318 well as *Ihh* in immature and mature AC and compared these patterns to the response when IFT88
319 was disrupted. Once again, we used confocal microscopy to image the FastRed detection and
320 overlaid these results with DIC to visualize cell morphology, the tidemark (Fig. 8, dashed blue
321 line), and the subchondral bone (sb, solid white line). First, we established patterning in
322 immature AC at 3 weeks. In control AC, *Gli1* and *Ptch1* were expressed in overlapping domains
323 surrounding the future tidemark in the first 3-4 cell layers in the femoral condyle (Fig. 8Aa-Ab)
324 and 4-6 cell layers from the surface in the tibial plateau (Fig. 8Ba-Bb). Importantly, these data
325 were consistent with those from our *Gli-LacZ* studies (Fig. 7A-B). In both regions only cells
326 juxtaposed to the underlying subchondral bone expressed *Ihh* (Fig 8Ac and Bc). Two things were
327 particularly notable about these patterns in immature AC: 1- the location of the future tidemark
328 correlated strongly with *Gli1* and *Ptch1* expression, and 2- despite the *Ihh*-expressing cells being
329 located always nearest the subchondral bone, the responding cells were closer to the surface in
330 condylar cartilage than in the tibial plateau. In mutant AC at this stage, *Gli1* was significantly
331 reduced in both femoral condyle and tibial plateau AC (Fig. 8Ad and Bd), consistent with *Gli1-*
332 *LacZ* studies (Fig. 7C-D). *Ptch1* expression generally followed the same profile, but with some
333 notable groups of positive cells in the femoral condyle (Fig. 8Ae, arrows and Be). Importantly,
334 *Ihh* expression was unchanged compared to controls (Fig. 8Af and Bf). Thus, down regulation of
335 signaling in this context is due to lack of response rather than lack of ligand expression.
336 We performed identical analyses in mature AC at 8 weeks of age. Femoral condyle AC of
337 controls displayed *Gli1* expression in non-mineralized chondrocytes including surface zone cells
338 (Fig. 8Ca), *Ptch1* expression in cells at the level of the tidemark (Fig. 8Cb), and *Ihh* expression
339 in mineralized chondrocytes beneath the tidemark (Fig. 8Cc). Tibial plateau AC displayed

340 overlapping *Gli1* and *Ptch1* in a zone 2-3 cell layers thick surrounding the tidemark (Fig. 8Da-b)
341 and *Ihh* in mineralized chondrocytes beneath the tidemark (Fig. 8Dc). Femoral condyle cartilage
342 of mutants displayed generally reduced *Gli1* above the tidemark (Fig. 8Cd) consistent with *Gli1-*
343 *LacZ* studies. Interestingly, while *Ptch1* was also significantly reduced compared to control
344 cartilage, the random distribution of persistent *Ptch1*-expressing chondrocytes correlated with
345 the irregularly shaped tidemark (Fig. 8Ce, arrows). *Ihh* also persisted but was ectopically
346 expressing in some non-mineralized chondrocytes (Fig. 8Cf, arrows). In tibial plateau cartilage,
347 *Gli1* and *Ptch1* expression was highly increased in the load-bearing region (Fig. 8Dd-De)
348 consistent with *Gli1-LacZ,* but unlike the condylar cartilage, *Ihh* remained exclusively expressed
349 by non-mineralized chondrocytes beneath the tidemark (Fig.8Df). Taken together, these results
350 provide evidence that hedgehog gradients coordinate tidemark patterning and that primary cilia
351 guide zonal responses to provide unique tissue structure able to withstand local mechanical load.
352

353 **DISCUSSION**

354 Our study of joint-specific loss of primary cilia function (IFT88-flox) provides new and
355 probing insights into AC zonal patterning during postnatal development. We find that primary
356 cilia are dispensable for embryonic joint formation, in line with previous *in vivo* studies (Chang
357 et al., 2012; Irianto et al., 2014; Sheffield et al., 2018; Song et al., 2007; Yuan & Yang, 2015),
358 but we have now uncovered the fact that they function primarily for AC maturation between
359 adolescence (3 weeks) and adulthood (8 weeks). In this postnatal period, we discovered that the
360 loss of primary cilia in AC reduced cell density and altered chondrocyte fate in either
361 mineralized or non-mineralized cartilage, leading to disrupted ECM production/organization.
362 Our most important and surprising finding was that loss of IFT88 alters tidemark patterning and

363 topography in a manner mirroring alterations to hedgehog signaling. Through these analyses we
364 were also able to establish, for the first time, the spatial patterning of *Ihh* responsiveness in
365 mature AC.

366 Our study provides significant evidence that primary cilia and hedgehog signaling are key
367 regulators of tidemark formation in mature AC. Ihh is required for joint specification during
368 embryonic development (Koyama et al., 2007) and while the specific roles for hedgehog
369 signaling in postnatal life have not been fully clarified genetic over activation of hedgehog
370 signaling leads to early OA symptoms (Rockel et al., 2016). We show here that the emergence
371 and location of the future tidemark in developing AC correlates strongly with patterning from
372 Ihh signals. We show by RNAscope on tissue sections that even before the tidemark emerges at
373 3 weeks of age, hedgehog responding cells align with the future location of the tidemark in
374 mature AC. Thus, our data establish a key causative link between patterning of mineralized and
375 non-mineralized chondrocytes in AC and hedgehog signaling responses, guided by primary cilia.
376 In future work, the mechanisms linking hedgehog signaling to tidemark patterning should be
377 tested directly. Does the tidemark move dependent on a changing hedgehog response? What is
378 the response in tissue integrity? Interestingly, tidemark advancement and duplication have also
379 been associated with OA (Johnson, 1962; Lane & Bullough, 1980; Loeser et al., 2012; Oegema
380 et al., 1997; Radin et al., 1991). Thus, these studies would delineate whether the movement in the
381 tidemark advances the disease-state as hypothesized or serves another purpose yet to be
382 discovered.

383 Our data also provide novel evidence that AC hedgehog signaling regulates *prg4*
384 expression. *Prg4* (lubricin) is an important regulator of AC homeostasis (Das et al., 2019) and, in
385 particular, prevents tissue and matrix degradation that would lead to OA (Chavez et al., 2019;

386 Ruan et al., 2013). Understanding its transcriptional regulation may be key to preventing disease
387 progression. Previous work has provided evidence of *prg4* regulation via TGFβ (Chavez et al.,
388 2019), Creb5 (Zhang et al., 2021), Yap/Taz (Delve et al., 2020) and load-induced Cox2 (Abusara
389 et al., 2013; Ogawa et al., 2014). In our present study, the decreased response to Ihh signaling
390 detected in the non-mineralized chondrocytes of immature mutant AC was accompanied by
391 reductions of *Prg4*. In mature AC *prg4/Ihh* were maintained at low levels in the femoral condyle,
392 but expression of both genes increased dramatically in the load-bearing region of the tibial
393 plateau. While most tissues follow the dogma that loss of the primary cilia leads to loss of
394 hedghog signaling, the over-activation of hedgehog we see in our model is consistent with
395 studies of embryonic limb development (Haycraft et al., 2005; Huangfu & Anderson, 2005) and
396 postnatal musculoskeletal tissues (Chang et al., 2012; Kopinke et al., 2017) where Gli3 repressor
397 plays a larger role in tissue function. Here, we provide evidence that this over-activation also has
398 a mechanical loading component because only the load-bearing region of mature tibial plateau
399 cartilage displays excessive hedgehog response. It is also plausible that reduced production of
400 aggrecan and collagens might further compromise the response of chondrocytes to mechanical
401 loading, and increase in *Prg4*. Studies designed to alter mechanical load in this model or alter
402 hedgehog signaling separately would clarify the possible regulatory effect of hedgehog/load on
403 *Prg4* expression.
404 In addition to the patterning deficits already acknowledged, we also found significant
405 disruptions to the proteoglycan and collagen matrix in mutant animals. The overall mis-
406 patterning of *Col2a1*- and *Acan*-expressing cells in mature AC can likely be attributed to
407 hedgehog patterning disruptions that result in altered patterning of mineralized and non-
408 mineralized chondrocytes in mature AC. However, it is notable that changes to ECM gene

409 expression and production were not apparent in immature AC when hedgehog responsiveness
410 was already altered. For this reason, we explored TGFβ and BMP signaling in order to gain
411 further mechanistic insights into changes in ECM production in mature AC. We found that both
412 signaling pathways were unchanged at 3 weeks but were significantly altered at 8 weeks,
413 particularly in BMP signal response of the tibial plateau. Knowledge of the role(s) for BMP
414 signaling in postnatal AC are limited, but two studies of conditional ablation of either *Bmpr1a* or
415 *Bmp2* in embryonic joints (*Gdf5Cre*) reported no embryonic phenotype and a progressive loss of
416 ECM during postnatal stages without hypertrophy or loss of Sox9 (Gamer et al., 2018; Rountree
417 et al., 2004). These findings are strikingly similar to those we report here, particularly in the
418 load-bearing region of the tibial plateau where we also observe a reduction of pSmad159 at 8
419 weeks of age. Possibilities for the loss of BMP responsiveness might include an altered
420 adaptation to mechanical load without primary cilia or negative regulation by increased
421 hedgehog signaling in the same location. To the latter point, hedgehog signaling is a known
422 negative regulator of BMP during embryonic somitogenesis by enhancing the expression of
423 BMP antagonists Noggin and Gremlin (Murtaugh et al., 1999; Stafford et al., 2011). Perhaps, a
424 similar mechanism is at play here. In the femoral condyle, no such changes to BMP (or TGFβ)
425 are noted and we also could not detect major changes to *Col2a1* or *Acan* gene expression. We
426 believe that alterations to ECM in the femoral condyle are driven by cellular patterning defects
427 that result in altered ECM organization while tibial plateau cartilage displays reduced ECM due
428 to BMP/TGFβ dysregulation.

429 Our current study also raises new questions regarding the degree to which the primary
430 cilium (and more specifically, IFT88) is required for mechanical adaptation in chondrocytes *in*
431 *vivo*. *In vitro* studies of chondrocytes that lack primary cilia suggested a loss of mechanical

432 transduction (Deren et al., 2016; Wann et al., 2012). Our present study shows a differential tissue
433 response of hedgehog signaling in the femoral condyle and the load-bearing region of the tibial
434 plateau. This altered response to ambulation load is indicative that tibial plateau chondrocytes are
435 capable of "feeling" some mechanical load and have adapted without primary cilia. The
436 pericellular matrix plays a major role in articular chondrocyte mechanosensation (Guilak et al.,
437 2006; Wilusz et al., 2012). Mutant AC continues to display perlecan localization in non-
438 mineralized chondrocytes despite cellular mis-patterning that might account for the maintained
439 ability to adapt to mechanical load. Although the mechanical load response is altered in mutant
440 animals, the data highlight the fact that cells are capable of mechanosensation through multiple
441 mechanisms not necessarily requiring primary cilia.

442 On a broader level, our study underscores the differential topographical character of AC
443 in normal joints and the differential phenotype due to the loss of primary cilia during
444 development. Each joint must be uniquely fitted to the load-bearing and movement requirements
445 of each anatomic location, and our study provides evidence that tidemark patterning is involved
446 in this evolution. Specifically, we highlight differential tidemark patterning even in opposing AC
447 in the same joint and a differential response to the loss of primary cilia. Femoral condyle AC
448 showed more significant patterning disruptions, while tibial plateau AC showed more significant
449 ECM loss. In this context, it is interesting to note that the mutant femoral condyle still elicited a
450 significant reduction in mechanical stiffness. Our observations raise the important possibility that
451 tissue patterning plays a much more significant role in overall AC integrity than currently
452 appreciated. Taken into consideration and exploiting these facets of AC biology experimentally
453 could lead to creation of more effective strategies for cartilage regeneration and repair.
454

455 ## Material and Methods

456 **Animals.** All studies involving mice were reviewed by our institutional IACUC at The
457 Children's Hospital of Philadelphia. All animals were handled, treated and cared for according to
458 the approved protocols. *IFT88-flox* (Stock no. 022409) and *Rosa-TdTomato* mice (Stock no.
459 007914) were obtained from the Jackson Laboratory (Bar Harbor, ME, USA). *Gdf5Cre* mice
460 (kindly provided by Dr. D. Kingsley) were described previously (Rountree et al., 2004) and line
461 B was used in the present study. Wildtype littermate animals were used for controls.

462 **AFM-based nanoindentation.** AFM-nanoindentation was applied to freshly dissected femoral
463 condyle and tibial plateau cartilage from mice at 8 weeks of age (n = 5 animals), following the
464 established procedure (Doyran et al., 2017; Han et al., 2019). Immediately after euthanasia,
465 cartilage was dissected free of tendon and ligament tissues and glued onto AFM sample discs by
466 a cyanoacrylate adhesive gel (Loctite 409, Henkel Corp., Rocky Hill, CT, USA). Throughout the
467 procedure, tissues were immersed in PBS with protease inhibitors (Pierce 88266, Fisher
468 Scientific, Rockford, IL, USA) to minimize post- mortem degradation. Nano-indentation was
469 performed on the surfaces of cartilage on a Dimension Icon AFM (Bruker Nano, Santa Barbara,
470 CA, USA) using a colloidal AFM probe. The probe was custom-made by attaching a polystyrene
471 microsphere (R ≈ 12.5 μm, PolySciences, Warrington, PA) to a tipless cantilever (nominal k ≈
472 5.4 N/m, cantilever C, HQ:NSC35/tipless/Cr–Au, Nano-AndMore, Watsonville, C, USA) using
473 liquid epoxy glue (M-bond 610, SPI Supplies, West Chester, PA). For each sample, at least 10
474 random, different indentation locations were tested on each selected region of interest up to ~1
475 μN force at 10 μm/s AFM z-piezo displacement rate. The effective indentation modulus, E_{ind},
476 was calculated by fitting the entire loading portion of each indentation force delpth (F–D) curve

477 to the Hertz model, where R is the tip radius and ν is the Poisson's ratio (0.1 for cartilage
478 (Buschmann et al., 1999)).
479 **Tissue Processing.** Joints processed for frozen sectioning were injected with 4% PFA, fixed for
480 2 days at 4°C, decalcified in 20% EDTA for 6-10 days (depending on age), washed in PBS 3X15
481 minutes, equilibrated in 15% sucrose for 6-8 hours and in 30% sucrose for 16-36 hours
482 (depending on age) and embedded in OCT. Sections were either take at 18μm thick for normal
483 slide collection or 10 μm thick on Kawamoto's cryofilm (Kawamoto & Kawamoto, 2021) to
484 preserve tissue morphology. Joints processed for paraffin sectioning (basic histology and
485 immunofluorescence) were injected with 10% NBF, fixed for 2 days at 4°C, decalcified in 20%
486 EDTA for 6-10 days (depending on age), washed in PBS 3X15 minutes, washed in 70% ethanol
487 3X15min and processed to paraffin by automation overnight. Joints processed for RNAscope
488 (Advanced Cell Diagnostics, Inc., San Jose, CA), were also processed for paraffin sectioning
489 using Morse's solution for decalcification as previously described (de Charleroy et al., 2021). All
490 sections were cut at 6 μm thick and slides were prepared with mutant and littermate control
491 sections on a single slide for each probe (N = 5 per time point).
492 **Histology/Immunofluorescence.** Safranin O staining was performed using standard
493 protocols and imaged using a Nikon Nikon Eclipse Ci-L upright microscope with attached DS-
494 Fi3 camera (Nikon Corp., Tokyo, Japan). Immunofluorescence staining was carried out on
495 frozen or paraffin sections depending on antibody optimization. For staining on frozen section,
496 1X PBS + 0.1% tween was used for all washes and incubations. Sections were blocked with 5%
497 donkey serum and incubated overnight at 4°C against MMP13 (1:100, Abcam ab39012,
498 Cambridge, UK) and for 2 hours at room temperature with a Cy3-conjugated secondary (1:500,
499 Jackson Immunoresearch, West Grove, PA). For staining on paraffin sections antigen retrieval

500 was performed by either 1mg/ml trypsin (Sigma, T7168, St. Louis, MO) or 10 μg/ml Proteinase
501 K for 20 minutes at 37°C. For non-amplified staining, sections were blocked with 5% donkey
502 serum (and Mouse-on-Mouse block as necessary from Vector Laboratories, Inc., Burlingame,
503 CA) and incubated overnight at 4°C with an antibody against either Perlecan (1:50, Life
504 Technologies, MA1-06821, Carlsbad, CA), Collagen2a1 (1:50, MilliporeSigma, MAB8887,
505 Burlington, MA), CollagenX (1:50, MilliporeSigma, 234196), or acetylated tubulin (1:200,
506 MilliporeSigma, MAB8887) and for 2 hours at room temperature with Cy3- or AF488-
507 conjugated secondary antibodies (1:500, Jackson Immunoresearch). For amplified staining, all
508 incubations after antigen retrieval were performed at room temperature. 1X PBS + 0.1% triton
509 was used for permeabilization (20 minutes) and 1X PBS + 0.1% tween was used for all washes
510 and buffers. Sections were treated with 3.6% H2O2 (made from 30% stock in water), blocked
511 with 2.5-10% donkey serum (and Mouse-on-Mouse block as necessary from Vector
512 Laboratories), incubated for 90 minutes with an antibody against either Sox9 (1:2000, Novus
513 Biologicals, AF3075, Littleton, CO), Aggrecan (1:25, Developmental Studies Hybridoma Bank,
514 12/21/1-C-6, Iowa City, IA), pSmad2 (1:1500, Cell Signaling Technology, 3108S, Danvers, MA)
515 or pSmad159 (1:800, Cell Signaling Technologies, 13820), for 1 hour with biotin-conjugated
516 secondary antibodies (1:500, Jackson Immunoresearch), for 1 hour with Vectastain Elite ABC
517 amplification kit (Vector Laboratories, Inc.) and developed for 10 minutes with fluorescein- or
518 Cy3-conjugated Tyramide amplication system (Perkin Elmer, Shelton, CT). Amplified staining
519 for Aggrecan was performed without detergent (1X PBS only) and included the following
520 additional antigen retrieval steps prior to blocking: reduction with 10mM DTT for 2 hours at
521 37°C, alkylation with 40mM Iodoacetamide for 2 hours at room temperature, and 5 mg/ml
522 Hyaluronidase (in 10% serum) for 1 hour at 37°C. All sections were counterstained with DAPI

523 (1 mg/ml stock per manufacturer guidelines, Sigma, D9542) diluted 1:10,000 in wash buffer for
524 10 minutes and coverslipped using Prolong Gold (Invitrogen, P36930, Waltham, MA). A Leica
525 DMi8CEL Advanced inverted SP8 confocal was used to collect fluorescent and DIC images
526 (Leica Camera, Wetzlar, Germany). All stains were performed on at least 5 mutants and
527 littermate controls per time point.

528 **Quantification from tissue sections.** All quantification was carried out using ImageJ
529 (National Institutes of Health, Software, Bethesda, MD) with FIJI plugins. All sections were
530 chosen from the central region of the medial knee. For AC thickness measurements, Safranin O-
531 stained sections were used. For each section (3-6 per animal), the thickest region of AC was
532 identified and 8 lines were drawn manually and measured. An average and standard error was
533 calculated from all lines in all sections per region of interest. For AC composition and cell
534 density measurements DIC images overlaid with DAPI were used. The % composition was
535 calculated by manually outlining and measuring the total cartilage, non-mineralized cartilage and
536 mineralized cartilage area from at least 2 sections per animal. Cell density of the non-mineralized
537 cartilage was calculated by counting (cell counter plugin) nuclei (DAPI in that area from at least
538 2 sections per animal. Density and %-positive cells for pSmad2 and pSmad159 were calculated
539 from immunofluorescent-stained slides counterstained with DAPI and additionally imaged with
540 DIC. DIC was used to outline the non-mineralized cartilage region per section (at least 2 sections
541 per animal) and cells were counted using DAPI and pSmad staining.

542 **RNAscope.** RNAscope *in situ* hybridization was carried out using RNAscope2.5 HD Detection
543 reagent-RED (Advanced Cell Diagnostics, Newark, CA, USA) to visualize the spatio-temporal
544 expression of *Adamts4* (cat. #497161), *Adamts5* (cat. #427621), *Col2a1* (cat. #407221), *Acan*
545 (cat. #439101), *Prg4* (cat. #437661), *Gli1* (cat. #311001), *Ptch1* (cat. #402811), *Ihh* (cat.

546 #413091). Briefly, sections were pretreated with a custom reagent and the probe was hybridized
547 for 2 hours at 40°C in a custom oven. Signal was amplified with multiple reagents as per
548 manufacturer's protocols and final signal was detected and visualized by reaction with Fast Red
549 substrate for 10-20 minutes (dependent on age) at room temperature. Companion sections were
550 hybridized with positive (Cat No. 313911) or negative control probes (Cat. No. 310043) to
551 assure signaling specificity. Sections imaged with brightfield were counterstained with
552 hematoxylin, dried and sealed with Permount. Sections imaged with confocal microscopy were
553 counterstained with Hoescht and cover slipped with Prolong Gold. A Nikon Eclipse Ci-L upright
554 microscope with attached DS-Fi3 camera was used to capture brightfield images. A Leica
555 DMi8CEL Advanced inverted SP8 confocal was used to collect fluorescent and DIC images.
556 **Statistical Methodologies.** Data were analzed using Microsoft Excel and Prism 9 (Graphpad
557 Software, Inc., San Diego, CA). Student's *t* tests and one-way ANOVA was used to establish
558 statistical significance with a threshold set at $p < 0.05$.
559
560 **Acknowledgements:** This study was supported by NIH grants NIH/NIAMS F32AR074227 (to
561 D.R.), R01AR062908 (to M.P.), R01AR074490 (to L.H.) and P30AR069619 (to Penn Center for
562 Musculoskeletal Disorders). **Author Contributions:** D.R. and M.P. designed and managed the
563 study. D.R., K.H., C.C., and E.K. performed animal experiments, data analyses, imaging, and
564 quantifications. B.H. and L.H. performed AFM-nanoindentation and analysed data. D.R. wrote
565 the manuscript with contributions and input from all authors. **Competing Interests:** The authors
566 declare that they have no competing interests. **Data and material availability.** All data
567 associated with this study are present in the paper and available from corresponding author upon
568 reasonable request.

569 **REFERENCES**

570 Abusara, Z., Krawetz, R., Steele, B., DuVall, M., Schmidt, T., & Herzog, W. (2013). Muscular
571 loading of joints triggers cellular secretion of PRG4 into the joint fluid. *Journal of*
572 *Biomechanics*, *46*(7), 1225–1230. https://doi.org/10.1016/j.jbiomech.2013.02.027

573 Allen, B. L., Song, J. Y., Izzi, L., Althaus, I. W., Kang, J.-S., Charron, F., Krauss, R. S., &
574 McMahon, A. P. (2011). Overlapping roles and collective requirement for the coreceptors
575 GAS1, CDO, and BOC in SHH pathway function. *Developmental Cell*, *20*(6), 775–787.
576 https://doi.org/10.1016/j.devcel.2011.04.018

577 Allen, B. L., Tenzen, T., & McMahon, A. P. (2007). The Hedgehog-binding proteins Gas1 and
578 Cdo cooperate to positively regulate Shh signaling during mouse development. *Genes &*
579 *Development*, *21*(10), 1244–1257. https://doi.org/10.1101/gad.1543607

580 Anvarian, Z., Mykytyn, K., Mukhopadhyay, S., Pedersen, L. B., & Christensen, S. T. (2019).
581 Cellular signalling by primary cilia in development, organ function and disease. *Nature*
582 *Reviews. Nephrology*, *15*(4), 199–219. https://doi.org/10.1038/s41581-019-0116-9

583 Bae, J.-S., Gutierrez, S., Narla, R., Pratap, J., Devados, R., van Wijnen, A. J., Stein, J. L., Stein,
584 G. S., Lian, J. B., & Javed, A. (2007). Reconstitution of Runx2/Cbfa1-null cells identifies
585 a requirement for BMP2 signaling through a Runx2 functional domain during osteoblast
586 differentiation. *Journal of Cellular Biochemistry*, *100*(2), 434–449.
587 https://doi.org/10.1002/jcb.21039

588 Buschmann, M. D., Kim, Y. J., Wong, M., Frank, E., Hunziker, E. B., & Grodzinsky, A. J.
589 (1999). Stimulation of aggrecan synthesis in cartilage explants by cyclic loading is
590 localized to regions of high interstitial fluid flow. *Archives of Biochemistry and*
591 *Biophysics*, *366*(1), 1–7. https://doi.org/10.1006/abbi.1999.1197

592 Chang, C.-F., Ramaswamy, G., & Serra, R. (2012). Depletion of primary cilia in articular
593 chondrocytes results in reduced Gli3 repressor to activator ratio, increased Hedgehog
594 signaling, and symptoms of early osteoarthritis. *Osteoarthritis and Cartilage*, *20*(2), 152–
595 161. https://doi.org/10.1016/j.joca.2011.11.009
596 Chavez, R. D., Sohn, P., & Serra, R. (2019). Prg4 prevents osteoarthritis induced by dominant-
597 negative interference of TGF-ß signaling in mice. *PloS One*, *14*(1), e0210601.
598 https://doi.org/10.1371/journal.pone.0210601
599 Chen, C. G., Thuillier, D., Chin, E. N., & Alliston, T. (2012). Chondrocyte-intrinsic Smad3
600 represses Runx2-inducible matrix metalloproteinase 13 expression to maintain articular
601 cartilage and prevent osteoarthritis. *Arthritis and Rheumatism*, *64*(10), 3278–3289.
602 https://doi.org/10.1002/art.34566
603 Coles, J. M., Zhang, L., Blum, J. J., Warman, M. L., Jay, G. D., Guilak, F., & Zauscher, S.
604 (2010). Loss of cartilage structure, stiffness, and frictional properties in mice lacking
605 PRG4. *Arthritis and Rheumatism*, *62*(6), 1666–1674. https://doi.org/10.1002/art.27436
606 Cosden-Decker, R. S., Bickett, M. M., Lattermann, C., & MacLeod, J. N. (2012). Structural and
607 functional analysis of intra-articular interzone tissue in axolotl salamanders.
608 *Osteoarthritis and Cartilage*, *20*(11), 1347–1356.
609 https://doi.org/10.1016/j.joca.2012.07.002
610 Coveney, C. R., Collins, I., Mc Fie, M., Chanalaris, A., Yamamoto, K., & Wann, A. K. T.
611 (2018). Cilia protein IFT88 regulates extracellular protease activity by optimizing LRP-
612 1–mediated endocytosis. *The FASEB Journal*, *32*(12), 6771–6782.
613 https://doi.org/10.1096/fj.201800334

614 Das, N., Schmidt, T. A., Krawetz, R. J., & Dufour, A. (2019). Proteoglycan 4: From Mere
615 Lubricant to Regulator of Tissue Homeostasis and Inflammation: Does proteoglycan 4
616 have the ability to buffer the inflammatory response? *BioEssays: News and Reviews in*
617 *Molecular, Cellular and Developmental Biology*, *41*(1), e1800166.
618 https://doi.org/10.1002/bies.201800166
619 de Charleroy, C., Haseeb, A., & Lefebvre, V. (2021). Preparation of Adult Mouse Skeletal
620 Tissue Sections for RNA In Situ Hybridization. *Methods in Molecular Biology (Clifton,*
621 *N.J.)*, *2245*, 85–92. https://doi.org/10.1007/978-1-0716-1119-7_6
622 Decker, R. S. (2017). Articular cartilage and joint development from embryogenesis to
623 adulthood. *Seminars in Cell & Developmental Biology*, *62*, 50–56.
624 https://doi.org/10.1016/j.semcdb.2016.10.005
625 Decker, R. S., Um, H.-B., Dyment, N. A., Cottingham, N., Usami, Y., Enomoto-Iwamoto, M.,
626 Kronenberg, M. S., Maye, P., Rowe, D. W., Koyama, E., & Pacifici, M. (2017). Cell
627 origin, volume and arrangement are drivers of articular cartilage formation,
628 morphogenesis and response to injury in mouse limbs. *Developmental Biology*, *426*(1),
629 56–68. https://doi.org/10.1016/j.ydbio.2017.04.006
630 Delve, E., Co, V., Regmi, S. C., Parreno, J., Schmidt, T. A., & Kandel, R. A. (2020). YAP/TAZ
631 regulates the expression of proteoglycan 4 and tenascin C in superficial-zone
632 chondrocytes. *European Cells & Materials*, *39*, 48–64.
633 https://doi.org/10.22203/eCM.v039a03
634 Deren, M. E., Yang, X., Guan, Y., & Chen, Q. (2016). Biological and Chemical Removal of
635 Primary Cilia Affects Mechanical Activation of Chondrogenesis Markers in

636 Chondroprogenitors and Hypertrophic Chondrocytes. *International Journal of Molecular*
637 *Sciences*, *17*(2), 188. https://doi.org/10.3390/ijms17020188
638 Doyran, B., Tong, W., Li, Q., Jia, H., Zhang, X., Chen, C., Enomoto-Iwamoto, M., Lu, X. L.,
639 Qin, L., & Han, L. (2017). Nanoindentation Modulus of Murine Cartilage: A Sensitive
640 Indicator of the Initiation and Progression of Post-Traumatic Osteoarthritis.
641 *Osteoarthritis and Cartilage*, *25*(1), 108–117. https://doi.org/10.1016/j.joca.2016.08.008
642 Ferguson, C. M., Schwarz, E. M., Reynolds, P. R., Puzas, J. E., Rosier, R. N., & O'Keefe, R. J.
643 (2000). Smad2 and 3 mediate transforming growth factor-beta1-induced inhibition of
644 chondrocyte maturation. *Endocrinology*, *141*(12), 4728–4735.
645 https://doi.org/10.1210/endo.141.12.7848
646 Fujii, M., Takeda, K., Imamura, T., Aoki, H., Sampath, T. K., Enomoto, S., Kawabata, M., Kato,
647 M., Ichijo, H., & Miyazono, K. (1999). Roles of bone morphogenetic protein type I
648 receptors and Smad proteins in osteoblast and chondroblast differentiation. *Molecular*
649 *Biology of the Cell*, *10*(11), 3801–3813. https://doi.org/10.1091/mbc.10.11.3801
650 Gamer, L. W., Pregizer, S., Gamer, J., Feigenson, M., Ionescu, A., Li, Q., Han, L., & Rosen, V.
651 (2018). The Role of Bmp2 in the Maturation and Maintenance of the Murine Knee Joint.
652 *Journal of Bone and Mineral Research: The Official Journal of the American Society for*
653 *Bone and Mineral Research*, *33*(9), 1708–1717. https://doi.org/10.1002/jbmr.3441
654 Gannon, A. R., Nagel, T., Bell, A. P., Avery, N. C., & Kelly, D. J. (2015). Postnatal changes to
655 the mechanical properties of articular cartilage are driven by the evolution of its collagen
656 network. *European Cells & Materials*, *29*, 105–121; discussion 121-123.
657 https://doi.org/10.22203/ecm.v029a09

658 Goetz, S. C., & Anderson, K. V. (2010). The primary cilium: A signalling centre during
659 vertebrate development. *Nature Reviews. Genetics*, *11*(5), 331–344.
660 https://doi.org/10.1038/nrg2774
661 Guilak, F., Alexopoulos, L. G., Upton, M. L., Youn, I., Choi, J. B., Cao, L., Setton, L. A., &
662 Haider, M. A. (2006). The pericellular matrix as a transducer of biomechanical and
663 biochemical signals in articular cartilage. *Annals of the New York Academy of Sciences*,
664 *1068*, 498–512. https://doi.org/10.1196/annals.1346.011
665 Han, B., Li, Q., Wang, C., Patel, P., Adams, S. M., Doyran, B., Nia, H. T., Oftadeh, R., Zhou, S.,
666 Li, C. Y., Liu, X. S., Lu, X. L., Enomoto-Iwamoto, M., Qin, L., Mauck, R. L., Iozzo, R.
667 V., Birk, D. E., & Han, L. (2019). Decorin Regulates the Aggrecan Network Integrity and
668 Biomechanical Functions of Cartilage Extracellular Matrix. *ACS Nano*, *13*(10), 11320–
669 11333. https://doi.org/10.1021/acsnano.9b04477
670 Haseeb, A., Kc, R., Angelozzi, M., de Charleroy, C., Rux, D., Tower, R. J., Yao, L., Pellegrino
671 da Silva, R., Pacifici, M., Qin, L., & Lefebvre, V. (2021). SOX9 keeps growth plates and
672 articular cartilage healthy by inhibiting chondrocyte dedifferentiation/osteoblastic
673 redifferentiation. *Proceedings of the National Academy of Sciences of the United States*
674 *of America*, *118*(8), e2019152118. https://doi.org/10.1073/pnas.2019152118
675 Haycraft, C. J., Banizs, B., Aydin-Son, Y., Zhang, Q., Michaud, E. J., & Yoder, B. K. (2005).
676 Gli2 and Gli3 localize to cilia and require the intraflagellar transport protein polaris for
677 processing and function. *PLoS Genetics*, *1*(4), e53.
678 https://doi.org/10.1371/journal.pgen.0010053

679 Haycraft, C. J., Zhang, Q., Song, B., Jackson, W. S., Detloff, P. J., Serra, R., & Yoder, B. K.
680 (2007). Intraflagellar transport is essential for endochondral bone formation.
681 *Development*, *134*(2), 307–316. https://doi.org/10.1242/dev.02732
682 Holtz, A. M., Peterson, K. A., Nishi, Y., Morin, S., Song, J. Y., Charron, F., McMahon, A. P., &
683 Allen, B. L. (2013). Essential role for ligand-dependent feedback antagonism of
684 vertebrate hedgehog signaling by PTCH1, PTCH2 and HHIP1 during neural patterning.
685 *Development (Cambridge, England)*, *140*(16), 3423–3434.
686 https://doi.org/10.1242/dev.095083
687 Horiki, M., Imamura, T., Okamoto, M., Hayashi, M., Murai, J., Myoui, A., Ochi, T., Miyazono,
688 K., Yoshikawa, H., & Tsumaki, N. (2004). Smad6/Smurf1 overexpression in cartilage
689 delays chondrocyte hypertrophy and causes dwarfism with osteopenia. *The Journal of*
690 *Cell Biology*, *165*(3), 433–445. https://doi.org/10.1083/jcb.200311015
691 Huangfu, D., & Anderson, K. V. (2005). Cilia and Hedgehog responsiveness in the mouse.
692 *Proceedings of the National Academy of Sciences of the United States of America*,
693 *102*(32), 11325–11330. https://doi.org/10.1073/pnas.0505328102
694 Hunziker, E. B., Kapfinger, E., & Geiss, J. (2007). The structural architecture of adult
695 mammalian articular cartilage evolves by a synchronized process of tissue resorption and
696 neoformation during postnatal development. *Osteoarthritis and Cartilage*, *15*(4), 403–
697 413. https://doi.org/10.1016/j.joca.2006.09.010
698 Ionescu, A. M., Schwarz, E. M., Zuscik, M. J., Drissi, H., Puzas, J. E., Rosier, R. N., & O'Keefe,
699 R. J. (2003). ATF-2 cooperates with Smad3 to mediate TGF-beta effects on chondrocyte
700 maturation. *Experimental Cell Research*, *288*(1), 198–207. https://doi.org/10.1016/s0014-
701 4827(03)00181-2

Irianto, J., Ramaswamy, G., Serra, R., & Knight, M. M. (2014). Depletion of chondrocyte primary cilia reduces the compressive modulus of articular cartilage. *Journal of Biomechanics*, *47*(2), 579–582. https://doi.org/10.1016/j.jbiomech.2013.11.040

Javed, A., Afzal, F., Bae, J.-S., Gutierrez, S., Zaidi, K., Pratap, J., van Wijnen, A. J., Stein, J. L., Stein, G. S., & Lian, J. B. (2009). Specific residues of RUNX2 are obligatory for formation of BMP2-induced RUNX2-SMAD complex to promote osteoblast differentiation. *Cells, Tissues, Organs*, *189*(1–4), 133–137. https://doi.org/10.1159/000151719

Javed, A., Bae, J.-S., Afzal, F., Gutierrez, S., Pratap, J., Zaidi, S. K., Lou, Y., van Wijnen, A. J., Stein, J. L., Stein, G. S., & Lian, J. B. (2008). Structural coupling of Smad and Runx2 for execution of the BMP2 osteogenic signal. *The Journal of Biological Chemistry*, *283*(13), 8412–8422. https://doi.org/10.1074/jbc.M705578200

Johnson, L. (1962). *Joint remodeling as the basis for osteoarthritis*. *141*, 1237–1241.

Julkunen, P., Harjula, T., Iivarinen, J., Marjanen, J., Seppänen, K., Närhi, T., Arokoski, J., Lammi, M. J., Brama, P. A., Jurvelin, J. S., & Helminen, H. J. (2009). Biomechanical, biochemical and structural correlations in immature and mature rabbit articular cartilage. *Osteoarthritis and Cartilage*, *17*(12), 1628–1638. https://doi.org/10.1016/j.joca.2009.07.002

Kang, J. S., Alliston, T., Delston, R., & Derynck, R. (2005). Repression of Runx2 function by TGF-beta through recruitment of class II histone deacetylases by Smad3. *The EMBO Journal*, *24*(14), 2543–2555. https://doi.org/10.1038/sj.emboj.7600729

723 Kawamoto, T., & Kawamoto, K. (2021). Preparation of Thin Frozen Sections from Nonfixed and
724 Undecalcified Hard Tissues Using Kawamoto's Film Method. *Methods in Molecular*
725 *Biology (Clifton, N.J.)*, *2230*, 259–281. https://doi.org/10.1007/978-1-0716-1028-2_15
726 Kim, K.-O., Sampson, E. R., Maynard, R. D., O'Keefe, R. J., Chen, D., Drissi, H., Rosier, R. N.,
727 Hilton, M. J., & Zuscik, M. J. (2012). Ski inhibits TGF-β/phospho-Smad3 signaling and
728 accelerates hypertrophic differentiation in chondrocytes. *Journal of Cellular*
729 *Biochemistry*, *113*(6), 2156–2166. https://doi.org/10.1002/jcb.24089
730 Kopinke, D., Roberson, E. C., & Reiter, J. F. (2017). Ciliary Hedgehog Signaling Restricts
731 Injury-Induced Adipogenesis. *Cell*, *170*(2), 340-351.e12.
732 https://doi.org/10.1016/j.cell.2017.06.035
733 Koyama, E., Shibukawa, Y., Nagayama, M., Sugito, H., Young, B., Yuasa, T., Okabe, T.,
734 Ochiai, T., Kamiya, N., Rountree, R. B., Kingsley, D. M., Iwamoto, M., Enomoto-
735 Iwamoto, M., & Pacifici, M. (2008). A distinct cohort of progenitor cells participates in
736 synovial joint and articular cartilage formation during mouse limb skeletogenesis.
737 *Developmental Biology*, *316*(1), 62–73. https://doi.org/10.1016/j.ydbio.2008.01.012
738 Koyama, E., Young, B., Shibukawa, Y., Nagayama, M., Enomoto-Iwamoto, M., Iwamoto, M.,
739 Maeda, Y., Lanske, B., Song, B., Serra, R., & Pacifici, M. (2007). Conditional Kif3a
740 ablation causes abnormal hedgehog signaling topography, growth plate dysfunction and
741 ectopic cartilage formation in mouse cranial base synchondroses. *Development*
742 *(Cambridge, England)*, *134*(11), 2159–2169. https://doi.org/10.1242/dev.001586
743 Kozhemyakina, E., Zhang, M., Ionescu, A., Ayturk, U. M., Ono, N., Kobayashi, A., Kronenberg,
744 H., Warman, M. L., & Lassar, A. B. (2015). Identification of a Prg4-expressing articular

745 cartilage progenitor cell population in mice. *Arthritis & Rheumatology (Hoboken, N.J.)*,
746 *67*(5), 1261–1273. https://doi.org/10.1002/art.39030
747 Kronenberg, H. M. (2006). PTHrP and skeletal development. *Annals of the New York Academy*
748 *of Sciences*, *1068*, 1–13. https://doi.org/10.1196/annals.1346.002
749 Kvist, A. J., Nyström, A., Hultenby, K., Sasaki, T., Talts, J. F., & Aspberg, A. (2008). The major
750 basement membrane components localize to the chondrocyte pericellular matrix—A
751 cartilage basement membrane equivalent? *Matrix Biology: Journal of the International*
752 *Society for Matrix Biology*, *27*(1), 22–33. https://doi.org/10.1016/j.matbio.2007.07.007
753 Lane, L. B., & Bullough, P. G. (1980). Age-related changes in the thickness of the calcified zone
754 and the number of tidemarks in adult human articular cartilage. *The Journal of Bone and*
755 *Joint Surgery. British Volume*, *62*(3), 372–375. https://doi.org/10.1302/0301-
756 620X.62B3.7410471
757 Leboy, P., Grasso-Knight, G., D'Angelo, M., Volk, S. W., Lian, J. V., Drissi, H., Stein, G. S., &
758 Adams, S. L. (2001). Smad-Runx interactions during chondrocyte maturation. *The*
759 *Journal of Bone and Joint Surgery. American Volume*, *83-A Suppl 1*(Pt 1), S15-22.
760 Lefebvre, V., Angelozzi, M., & Haseeb, A. (2019). SOX9 in cartilage development and disease.
761 *Current Opinion in Cell Biology*, *61*, 39–47. https://doi.org/10.1016/j.ceb.2019.07.008
762 Li, L., Newton, P. T., Bouderlique, T., Sejnohova, M., Zikmund, T., Kozhemyakina, E., Xie, M.,
763 Krivanek, J., Kaiser, J., Qian, H., Dyachuk, V., Lassar, A. B., Warman, M. L., Barenius,
764 B., Adameyko, I., & Chagin, A. S. (2017). Superficial cells are self-renewing
765 chondrocyte progenitors, which form the articular cartilage in juvenile mice. *FASEB*
766 *Journal: Official Publication of the Federation of American Societies for Experimental*
767 *Biology*, *31*(3), 1067–1084. https://doi.org/10.1096/fj.201600918R

768 Li, T.-F., Gao, L., Sheu, T.-J., Sampson, E. R., Flick, L. M., Konttinen, Y. T., Chen, D.,
769 Schwarz, E. M., Zuscik, M. J., Jonason, J. H., & O'Keefe, R. J. (2010). Aberrant
770 hypertrophy in Smad3-deficient murine chondrocytes is rescued by restoring
771 transforming growth factor beta-activated kinase 1/activating transcription factor 2
772 signaling: A potential clinical implication for osteoarthritis. *Arthritis and Rheumatism*,
773 *62*(8), 2359–2369. https://doi.org/10.1002/art.27537
774 Loeser, R. F., Goldring, S. R., Scanzello, C. R., & Goldring, M. B. (2012). Osteoarthritis: A
775 disease of the joint as an organ. *Arthritis and Rheumatism*, *64*(6), 1697–1707.
776 https://doi.org/10.1002/art.34453
777 Longobardi, L., Li, T., Tagliafierro, L., Temple, J. D., Willcockson, H. H., Ye, P., Esposito, A.,
778 Xu, F., & Spagnoli, A. (2015). Synovial joints: From development to homeostasis.
779 *Current Osteoporosis Reports*, *13*(1), 41–51. https://doi.org/10.1007/s11914-014-0247-7
780 Marcelino, J., Carpten, J. D., Suwairi, W. M., Gutierrez, O. M., Schwartz, S., Robbins, C., Sood,
781 R., Makalowska, I., Baxevanis, A., Johnstone, B., Laxer, R. M., Zemel, L., Kim, C. A.,
782 Herd, J. K., Ihle, J., Williams, C., Johnson, M., Raman, V., Alonso, L. G., … Warman,
783 M. L. (1999). CACP, encoding a secreted proteoglycan, is mutated in camptodactyly-
784 arthropathy-coxa vara-pericarditis syndrome. *Nature Genetics*, *23*(3), 319–322.
785 https://doi.org/10.1038/15496
786 McGlashan, S. R., Cluett, E. C., Jensen, C. G., & Poole, C. A. (2008). Primary cilia in
787 osteoarthritic chondrocytes: From chondrons to clusters. *Developmental Dynamics: An*
788 *Official Publication of the American Association of Anatomists*, *237*(8), 2013–2020.
789 https://doi.org/10.1002/dvdy.21501

Mow, V., & Ratcliffe, A. (1997). *Structure and Function of Articular Cartilage and Meniscus.* (2nd ed.). Lippincott-Raven.

Mow, V., & Sugalski, M. (2001). *Physiology of synovial joints and articular cartilage: Vol. E.G. Gonzales (Ed.)* (3rd ed.). Butterwoth Heinemann Pubs.

Murtaugh, L. C., Chyung, J. H., & Lassar, A. B. (1999). Sonic hedgehog promotes somitic chondrogenesis by altering the cellular response to BMP signaling. *Genes & Development*, *13*(2), 225–237. https://doi.org/10.1101/gad.13.2.225

Nomura, M., Sakitani, N., Iwasawa, H., Kohara, Y., Takano, S., Wakimoto, Y., Kuroki, H., & Moriyama, H. (2017). Thinning of articular cartilage after joint unloading or immobilization. An experimental investigation of the pathogenesis in mice. *Osteoarthritis and Cartilage*, *25*(5), 727–736. https://doi.org/10.1016/j.joca.2016.11.013

O'Connor, K. M. (1997). Unweighting accelerates tidemark advancement in articular cartilage at the knee joint of rats. *Journal of Bone and Mineral Research: The Official Journal of the American Society for Bone and Mineral Research*, *12*(4), 580–589. https://doi.org/10.1359/jbmr.1997.12.4.580

Oegema, T. R., Carpenter, R. J., Hofmeister, F., & Thompson, R. C. (1997). The interaction of the zone of calcified cartilage and subchondral bone in osteoarthritis. *Microscopy Research and Technique*, *37*(4), 324–332. https://doi.org/10.1002/(SICI)1097-0029(19970515)37:4<324::AID-JEMT7>3.0.CO;2-K

Ogawa, H., Kozhemyakina, E., Hung, H.-H., Grodzinsky, A. J., & Lassar, A. B. (2014). Mechanical motion promotes expression of Prg4 in articular cartilage via multiple CREB-dependent, fluid flow shear stress-induced signaling pathways. *Genes & Development*, *28*(2), 127–139. https://doi.org/10.1101/gad.231969.113

813 Phimphilai, M., Zhao, Z., Boules, H., Roca, H., & Franceschi, R. T. (2006). BMP signaling is
814 required for RUNX2-dependent induction of the osteoblast phenotype. *Journal of Bone*
815 *and Mineral Research: The Official Journal of the American Society for Bone and*
816 *Mineral Research*, *21*(4), 637–646. https://doi.org/10.1359/jbmr.060109
817 Radin, E. L., Burr, D. B., Caterson, B., Fyhrie, D., Brown, T. D., & Boyd, R. D. (1991).
818 Mechanical determinants of osteoarthrosis. *Seminars in Arthritis and Rheumatism*, *21*(3
819 Suppl 2), 12–21. https://doi.org/10.1016/0049-0172(91)90036-y
820 Rhee, D. K., Marcelino, J., Baker, M., Gong, Y., Smits, P., Lefebvre, V., Jay, G. D., Stewart, M.,
821 Wang, H., Warman, M. L., & Carpten, J. D. (2005). The secreted glycoprotein lubricin
822 protects cartilage surfaces and inhibits synovial cell overgrowth. *Journal of Clinical*
823 *Investigation*, *115*(3), 622–631. https://doi.org/10.1172/JCI200522263
824 Ribes, V., & Briscoe, J. (2009). Establishing and interpreting graded Sonic Hedgehog signaling
825 during vertebrate neural tube patterning: The role of negative feedback. *Cold Spring*
826 *Harbor Perspectives in Biology*, *1*(2), a002014.
827 https://doi.org/10.1101/cshperspect.a002014
828 Rockel, J. S., Yu, C., Whetstone, H., Craft, A. M., Reilly, K., Ma, H., Tsushima, H., Puviindran,
829 V., Al-Jazrawe, M., Keller, G. M., & Alman, B. A. (2016). Hedgehog inhibits β-catenin
830 activity in synovial joint development and osteoarthritis. *The Journal of Clinical*
831 *Investigation*, *126*(5), 1649–1663. https://doi.org/10.1172/JCI80205
832 Rountree, R. B., Schoor, M., Chen, H., Marks, M. E., Harley, V., Mishina, Y., & Kingsley, D.
833 M. (2004). BMP Receptor Signaling Is Required for Postnatal Maintenance of Articular
834 Cartilage. *PLoS Biology*, *2*(11). https://doi.org/10.1371/journal.pbio.0020355

835 Ruan, M. Z., Erez, A., Guse, K., Dawson, B., Bertin, T., Chen, Y., Jiang, M.-M., Yustein, J.,
836 Gannon, F., & Lee, B. H. (2013). PROTEOGLYCAN 4 EXPRESSION PROTECTS
837 AGAINST THE DEVELOPMENT OF OSTEOARTHRITIS. *Science Translational*
838 *Medicine*, *5*(176), 176ra34. https://doi.org/10.1126/scitranslmed.3005409
839 Rux, D. R., Decker, R. S., Koyama, E., & Pacifici, M. (2019). Joints in the appendicular
840 skeleton: Developmental mechanisms and evolutionary influences. *Current Topics in*
841 *Developmental Biology*, *133*, 119–151. https://doi.org/10.1016/bs.ctdb.2018.11.002
842 Seo, H.-S., & Serra, R. (2007). Deletion of Tgfbr2 in Prx1-cre expressing mesenchyme results in
843 defects in development of the long bones and joints. *Developmental Biology*, *310*(2),
844 304–316. https://doi.org/10.1016/j.ydbio.2007.07.040
845 Serra, R. (2008). Role of Intraflagellar Transport and Primary Cilia in Skeletal Development.
846 *The Anatomical Record*, *291*(9), 1049–1061. https://doi.org/10.1002/ar.20634
847 Sheffield, I. D., McGee, M. A., Glenn, S. J., Baek, D. Y., Coleman, J. M., Dorius, B. K.,
848 Williams, C., Rose, B. J., Sanchez, A. E., Goodman, M. A., Daines, J. M., Eggett, D. L.,
849 Sheffield, V. C., Suli, A., & Kooyman, D. L. (2018). Osteoarthritis-Like Changes in
850 Bardet–Biedl Syndrome Mutant Ciliopathy Mice (Bbs1M390R/M390R): Evidence for a
851 Role of Primary Cilia in Cartilage Homeostasis and Regulation of Inflammation.
852 *Frontiers in Physiology*, *9*. https://doi.org/10.3389/fphys.2018.00708
853 Song, B., Haycraft, C. J., Seo, H., Yoder, B. K., & Serra, R. (2007). Development of the post-
854 natal growth plate requires intraflagellar transport proteins. *Developmental Biology*,
855 *305*(1), 202–216. https://doi.org/10.1016/j.ydbio.2007.02.003
856 Stafford, D. A., Brunet, L. J., Khokha, M. K., Economides, A. N., & Harland, R. M. (2011).
857 Cooperative activity of noggin and gremlin 1 in axial skeleton development.

858 *Development (Cambridge, England)*, *138*(5), 1005–1014.
859 https://doi.org/10.1242/dev.051938
860 St-Jacques, B., Hammerschmidt, M., & McMahon, A. P. (1999). Indian hedgehog signaling
861 regulates proliferation and differentiation of chondrocytes and is essential for bone
862 formation. *Genes & Development*, *13*(16), 2072–2086.
863 https://doi.org/10.1101/gad.13.16.2072
864 Thielen, N. G. M., van der Kraan, P. M., & van Caam, A. P. M. (2019). TGFβ/BMP Signaling
865 Pathway in Cartilage Homeostasis. *Cells*, *8*(9), E969.
866 https://doi.org/10.3390/cells8090969
867 Tomiya, M., Fujikawa, K., Ichimura, S., Kikuchi, T., Yoshihara, Y., & Nemoto, K. (2009).
868 Skeletal unloading induces a full-thickness patellar cartilage defect with increase of
869 urinary collagen II CTx degradation marker in growing rats. *Bone*, *44*(2), 295–305.
870 https://doi.org/10.1016/j.bone.2008.10.038
871 Wann, A. K. T., Zuo, N., Haycraft, C. J., Jensen, C. G., Poole, C. A., McGlashan, S. R., &
872 Knight, M. M. (2012). Primary cilia mediate mechanotransduction through control of
873 ATP-induced Ca2+ signaling in compressed chondrocytes. *FASEB Journal: Official*
874 *Publication of the Federation of American Societies for Experimental Biology*, *26*(4),
875 1663–1671. https://doi.org/10.1096/fj.11-193649
876 Wheway, G., Nazlamova, L., & Hancock, J. T. (2018). Signaling through the Primary Cilium.
877 *Frontiers in Cell and Developmental Biology*, *6*. https://doi.org/10.3389/fcell.2018.00008
878 Wilusz, R. E., Defrate, L. E., & Guilak, F. (2012). A biomechanical role for perlecan in the
879 pericellular matrix of articular cartilage. *Matrix Biology: Journal of the International*
880 *Society for Matrix Biology*, *31*(6), 320–327. https://doi.org/10.1016/j.matbio.2012.05.002

881 Yang, X., Chen, L., Xu, X., Li, C., Huang, C., & Deng, C. X. (2001). TGF-beta/Smad3 signals
882 repress chondrocyte hypertrophic differentiation and are required for maintaining
883 articular cartilage. *The Journal of Cell Biology*, *153*(1), 35–46.
884 https://doi.org/10.1083/jcb.153.1.35
885 Yuan, X., & Yang, S. (2015). Deletion of IFT80 Impairs Epiphyseal and Articular Cartilage
886 Formation Due to Disruption of Chondrocyte Differentiation. *PloS One*, *10*(6), e0130618.
887 https://doi.org/10.1371/journal.pone.0130618
888 Yuan, X., & Yang, S. (2016). Primary Cilia and Intraflagellar Transport Proteins in Bone and
889 Cartilage. *Journal of Dental Research*, *95*(12), 1341–1349.
890 https://doi.org/10.1177/0022034516652383
891 Zhang, C.-H., Gao, Y., Jadhav, U., Hung, H.-H., Holton, K. M., Grodzinsky, A. J., Shivdasani,
892 R. A., & Lassar, A. B. (2021). Creb5 establishes the competence for Prg4 expression in
893 articular cartilage. *Communications Biology*, *4*(1), 332. https://doi.org/10.1038/s42003-
894 021-01857-0
895
896

897 **FIGURES**

898

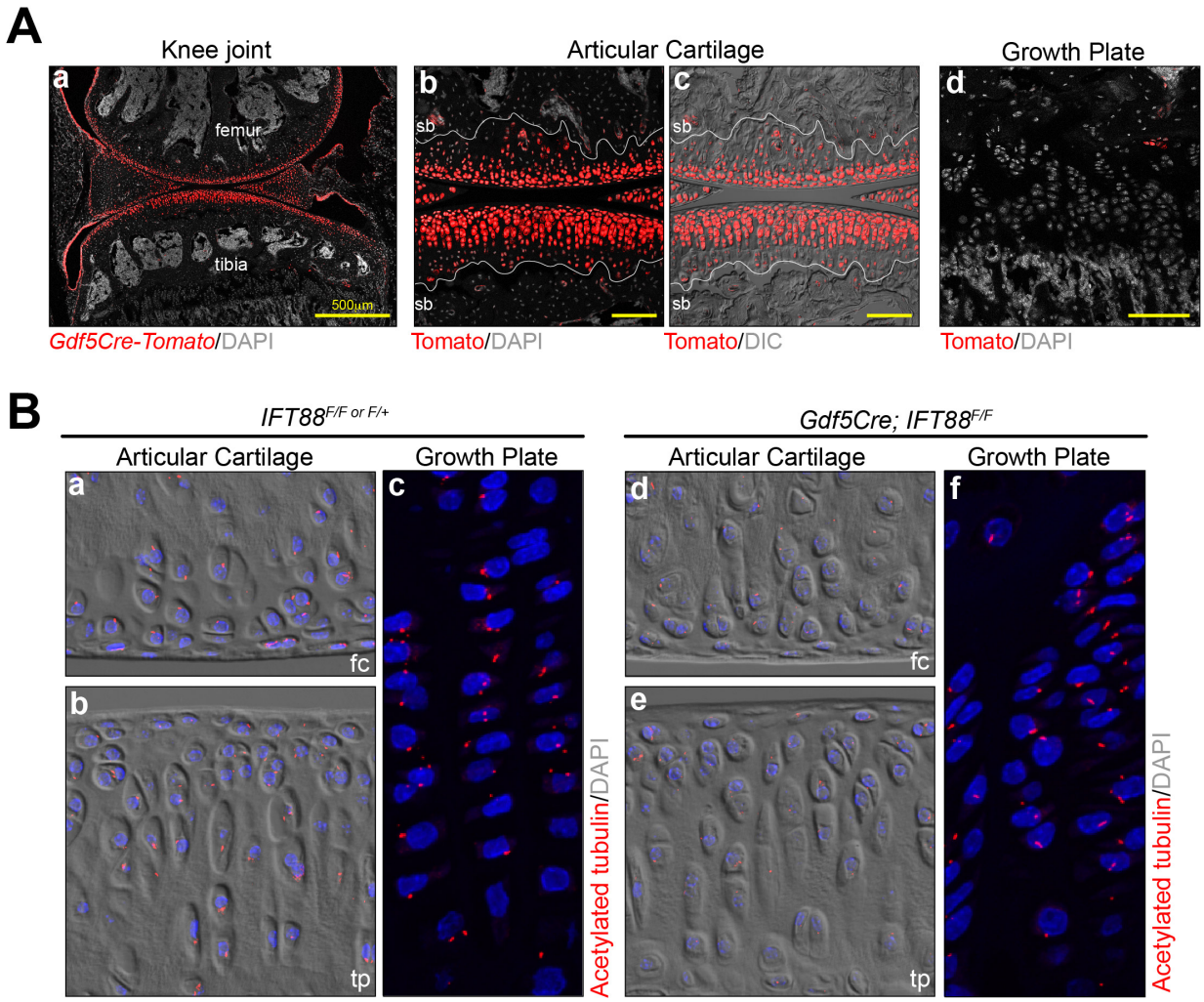

899

900 **Figure 1. *Gdf5Cre* is joint specific and its conditional deletion of *IFT88* results in loss of**

901 **primary cilia.** (**A**) *Gdf5Cre/+; Rosa-tdTomato* lineage cells are present in adult joints (a) and all

902 zones of AC as shown with DIC imaging to visualize the tidemark (b-c), but are absent in growth

903 plate (d). (**B**) Primary cilia are visualized by acetylated tubulin staining. They are present in

904 control AC (a-b) and growth plate chondrocytes (c); in mutants, they are absent from AC (d-e)

905 but still present in growth plate chondrocytes (f). sb, subchondral bone; fc, femoral condyle; tp,

906 tibial plateau. scale bar = 100 µm unless otherwise noted.

907

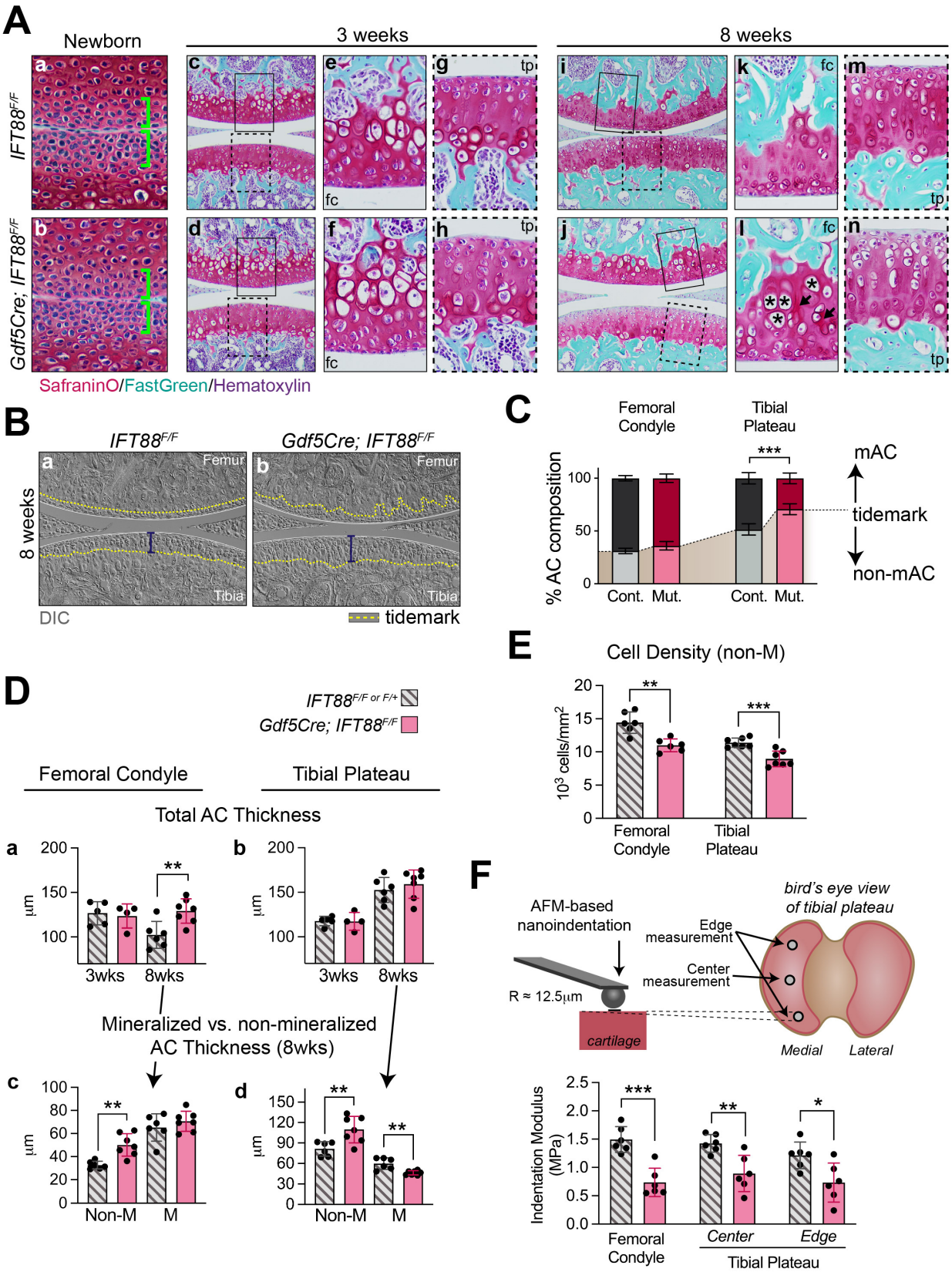
A
Newborn
3 weeks
8 weeks
IFT88F/F
Gdf5Cre; IFT88F/F
SafraninO/FastGreen/Hematoxylin
B
IFT88F/F
Gdf5Cre; IFT88F/F
8 weeks
Femur
Tibia
DIC
tidemark
C
Femoral Condyle
Tibial Plateau
% AC composition
mAC
tidemark
non-mAC
Cont. Mut. Cont. Mut.
D
IFT88F/F or F/+
Gdf5Cre; IFT88F/F
Femoral Condyle
Tibial Plateau
Total AC Thickness
3wks 8wks
Mineralized vs. non-mineralized AC Thickness (8wks)
Non-M M
E
Cell Density (non-M)
10³ cells/mm²
Femoral Condyle
Tibial Plateau
F
AFM-based nanoindentation
R ≈ 12.5μm
cartilage
bird's eye view of tibial plateau
Edge measurement
Center measurement
Medial
Lateral
Indentation Modulus (MPa)
Femoral Condyle
Center
Edge
Tibial Plateau

908

909 **Figure 2. Joint-specific deletion of *IFT88* results in disrupted AC tidemark patterning and**
910 **inferior biomechanical function.** (**A**) Safranin O staining at birth through 8 weeks. Nascent AC
911 at birth is unchanged in mutant joints (a-b, brackets). Low magnification (c-d) and high
912 magnification images of femoral condyle (e-f) or tibial plateau (g-h) are comparable in controls
913 and mutants at 3 weeks. At 8 weeks, control AC (i, k, m) displays strong safranin O staining
914 throughout the femoral condyle (k) and tibial plateau (m). In mutant AC (j, l, n), the femoral
915 condyle displays aberrant ECM deposition (l, arrows) and increased cell size (l, asterisks), while
916 the tibial plateau displays reduced Safranin O staining (n). (**B**) DIC imaging of the tidemark
917 (dashed yellow line) reveals ordered patterning in control AC (a). In mutant AC, the tidemark of
918 the femoral condyle is highly disorganized and its distance from the surface is increased in the
919 tibial plateau (b, bracket). (**C**) Mineralized (mAC) and non-mineralized (non-mAC) composition
920 is shown as a percent area from multiple tissue sections and is significantly altered in mutant
921 tibial plateau. (**D**) Measurements of AC height at the thickest point among tissue sections reveals
922 a significant increase in mutant femoral condyle at 8 weeks (a) but no change in tibial plateau
923 (b). Bisected into non-mineralized (non-M) and mineralized (M) thickness (c-d), mutants display
924 a thicker non-mineralized zone in both locations, and a reduced mineralized zone in the tibial
925 plateau. (**E**) Cell density in the non-mineralized AC is decreased in all knee joint AC. (**F**)
926 Biomechanical function was measured by AFM-nanoindentation from 3 regions. Schematic
927 shows approximate location of the 2 regions of tibial plateau AC. Indentation modulus was
928 significantly decreased in all locations. fc, femoral condyle; tp, tibial plateau scale bar = 100 μm.

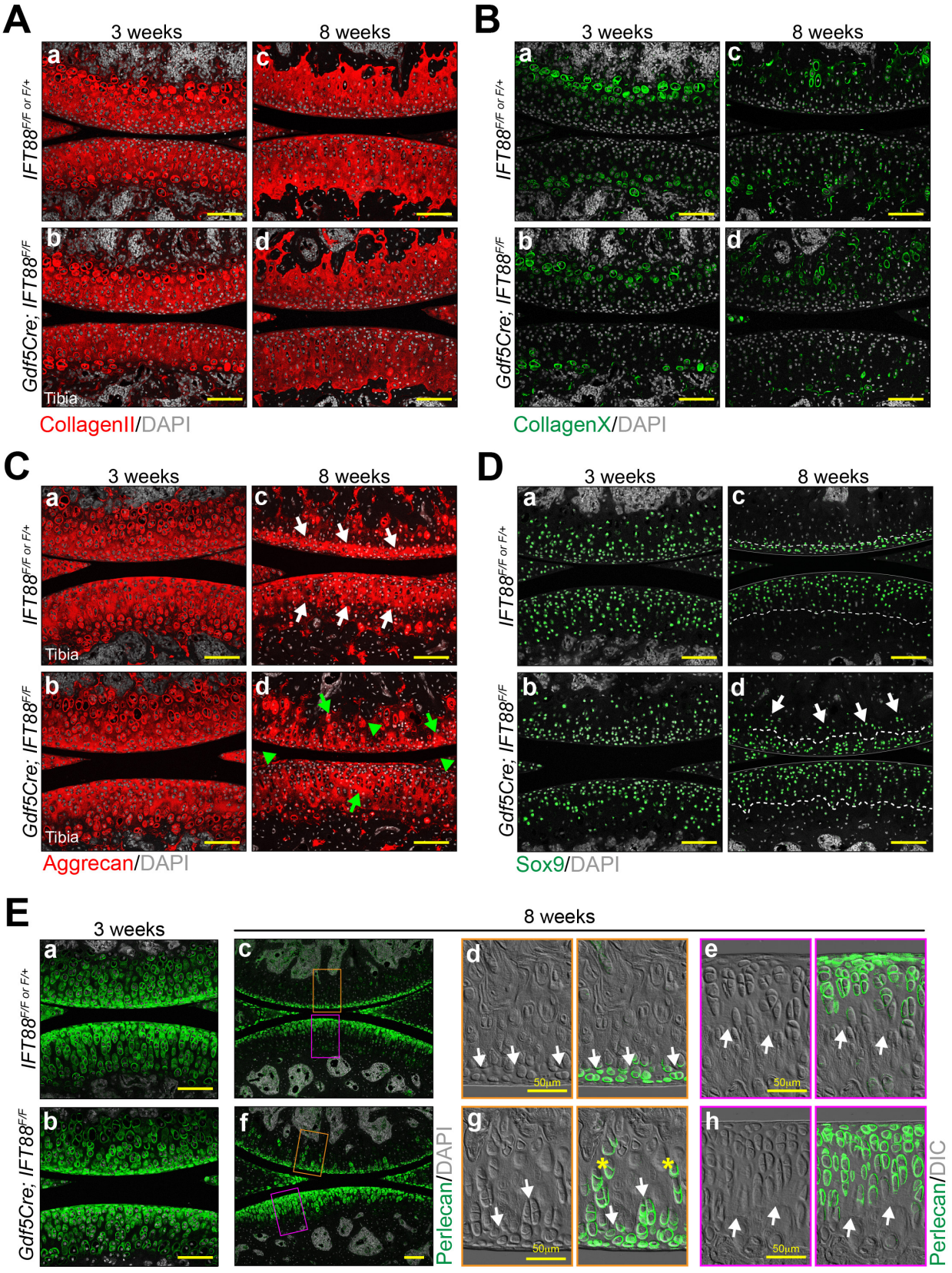
A
3 weeks
8 weeks
IFT88F/F or F/+
Gdf5Cre; IFT88F/F
Tibia
CollagenII/DAPI
B
CollagenX/DAPI
C
Aggrecan/DAPI
D
Sox9/DAPI
E
Perlecan/DAPI
Perlecan/DIC
50μm

929

930 **Figure 3. IFT88 regulates chondrocyte fate and matrix deposition in mineralized and non-**
931 **mineralized zones.** (**A**) Collagen II immunostaining is broadly distributed in AC and
932 comparable at 3 weeks (a-b) and moderately reduced at 8 weeks in mutants (c-d). (**B**) Collagen X
933 immunostaining is restricted to chondrocytes near the subchondral bone and is comparable at 3
934 weeks (a-b) and 8 weeks in all samples (c-d). (**C**) Aggrecan immunostaining is broadly
935 distributed and comparable at 3 weeks (a-b). It is enriched in non-mineralized 8 week AC of
936 controls (c, white arrows point to tidemark) and is disorganized in 8 week AC of mutants (d),
937 with random areas of high staining (green arrows) and low staining (green arrow heads). (**D**) Sox
938 9 is broadly distributed and comparable in AC at 3 weeks (a-b). It is also broadly distributed in
939 non-mineralized AC of controls and mutants at 8 weeks (c-d, dashed line represents the
940 tidemark), but mutant femoral condyle AC also displays ectopic Sox9-positive cells beyond the
941 tidemark (d, white arrows). (**E**) Perlecan is broadly distributed in AC and comparable at 3 weeks
942 (a-b) and is enriched nearest the surface at 8 weeks (c, f). High magnification with DIC shows
943 the tidemark (d, e, g, h, white arrows). Perlecan+ cells are present below the tidemark in mutant
944 femoral condyle (g, asterisks) and in deeper cell layers of mutant tibial plateau (h). scale bar =
945 100 μm.

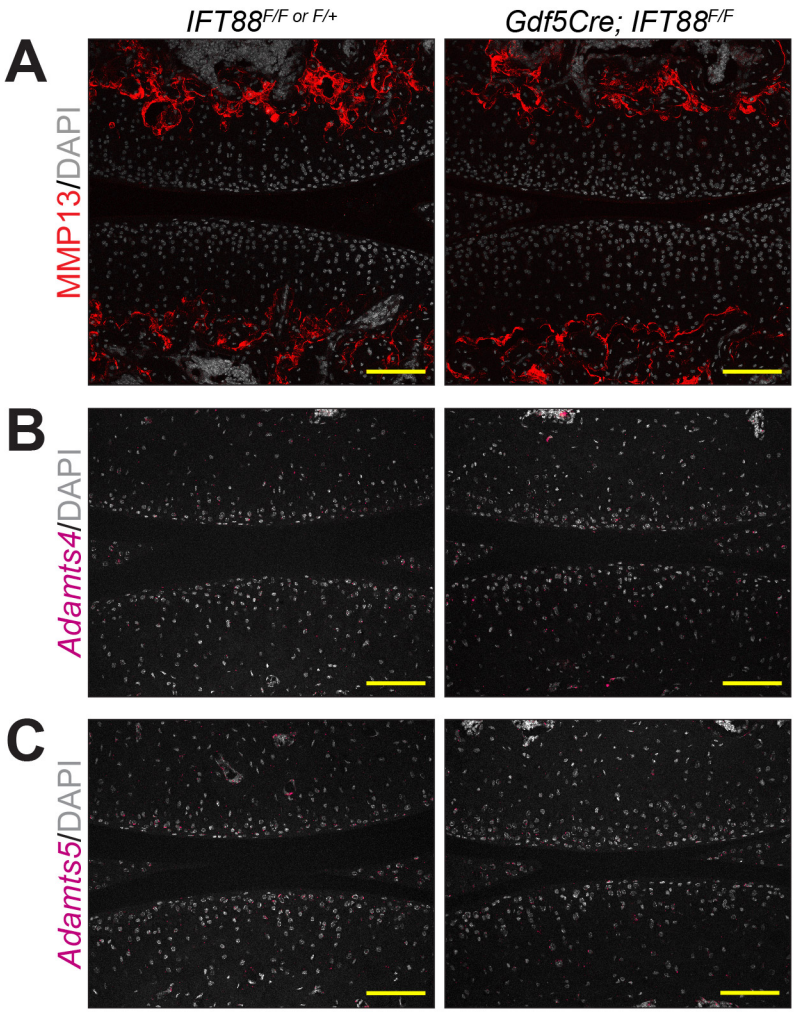

946

947 **Figure 4. Loss of IFT88 in AC does not increase degradation at 8 weeks.**

948 (**A**) Immunofluorescence for MMP13 is unchanged in controls and mutants and is always

949 restricted to subchondral bone. (**B-C**) *Adamts4* and *Adamts5* are not detectable in control or

950 mutant AC. scale bar = 100 µm.

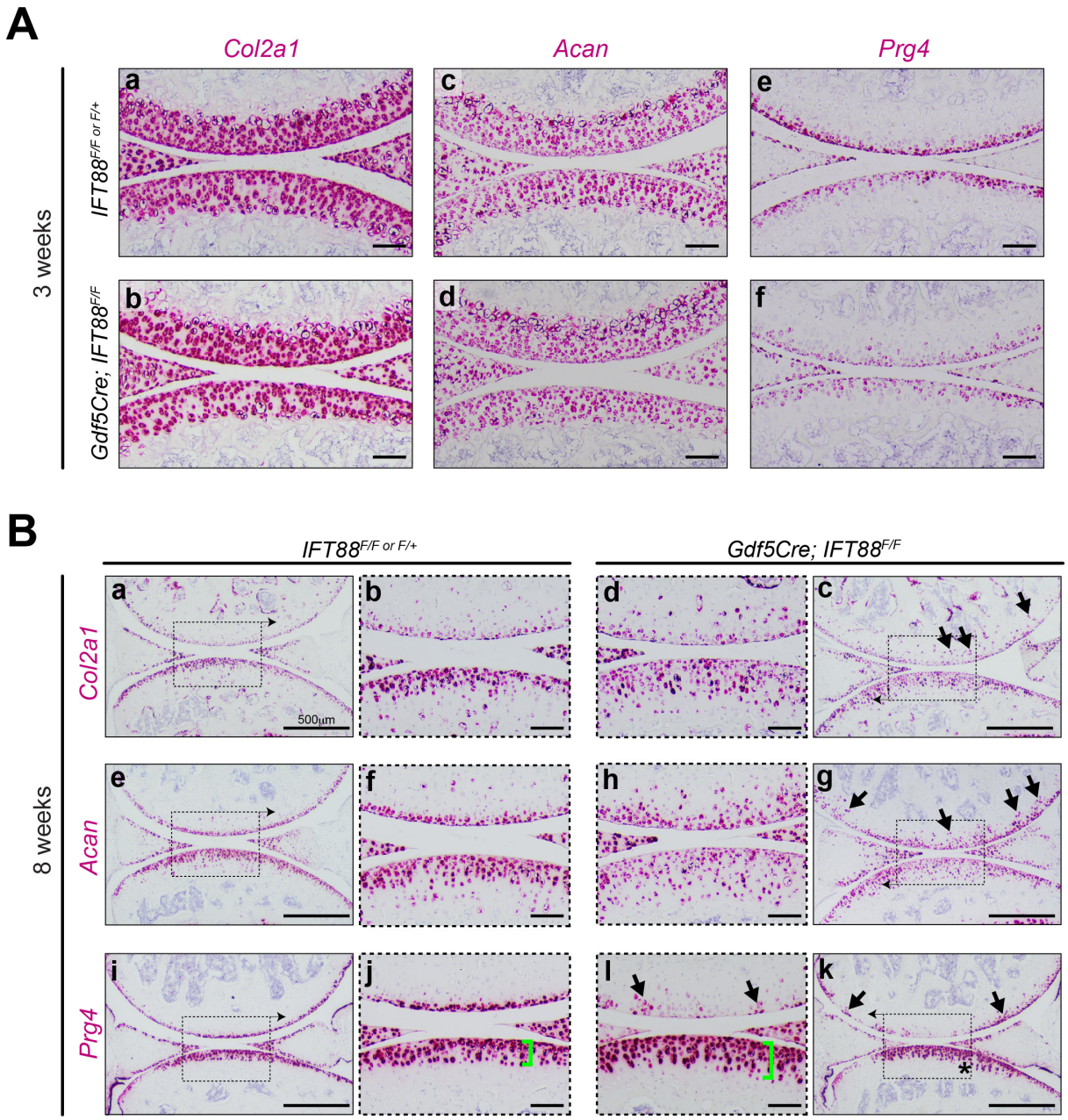

951

952 **Figure 5. Altered ECM in mature mutant AC are the result of transcriptional changes.**

953 (**A**) RNAscope at 3 weeks shows *Col2a1* (a-b) and *Acan* (c-d) are comparable in controls and

954 mutants. *Prg4* at 3 weeks is expressed close to the surface in control AC (e) and is broadly

955 reduced in mutant tissues (f). (**B**) RNAscope at 8 weeks. Low magnification images of *Col2a1*

956 (a) and *Acan* (e) show organization of control AC and high magnification images (b, f) depict

957 high levels of expression of both genes. Low magnification images of *Col2a1* (c) and *Acan* (g)
958 show disorganization in mutant AC, particularly in the femoral condyle (arrows). High
959 magnification images (d, h) highlight similar levels of expression to controls (b,f) in femoral
960 condyle but decreased expression in tibial plateau AC. *Prg4* in control AC is highly expressed
961 near the surface (i-j). *Prg4* expression in mutant AC (k-l) is decreased and patchy in the femoral
962 condyle (arrows), while it is increased and expressed more broadly in mutant tibial plateau
963 compared to control (asterisk and bracket). scale bar = 100 µm.

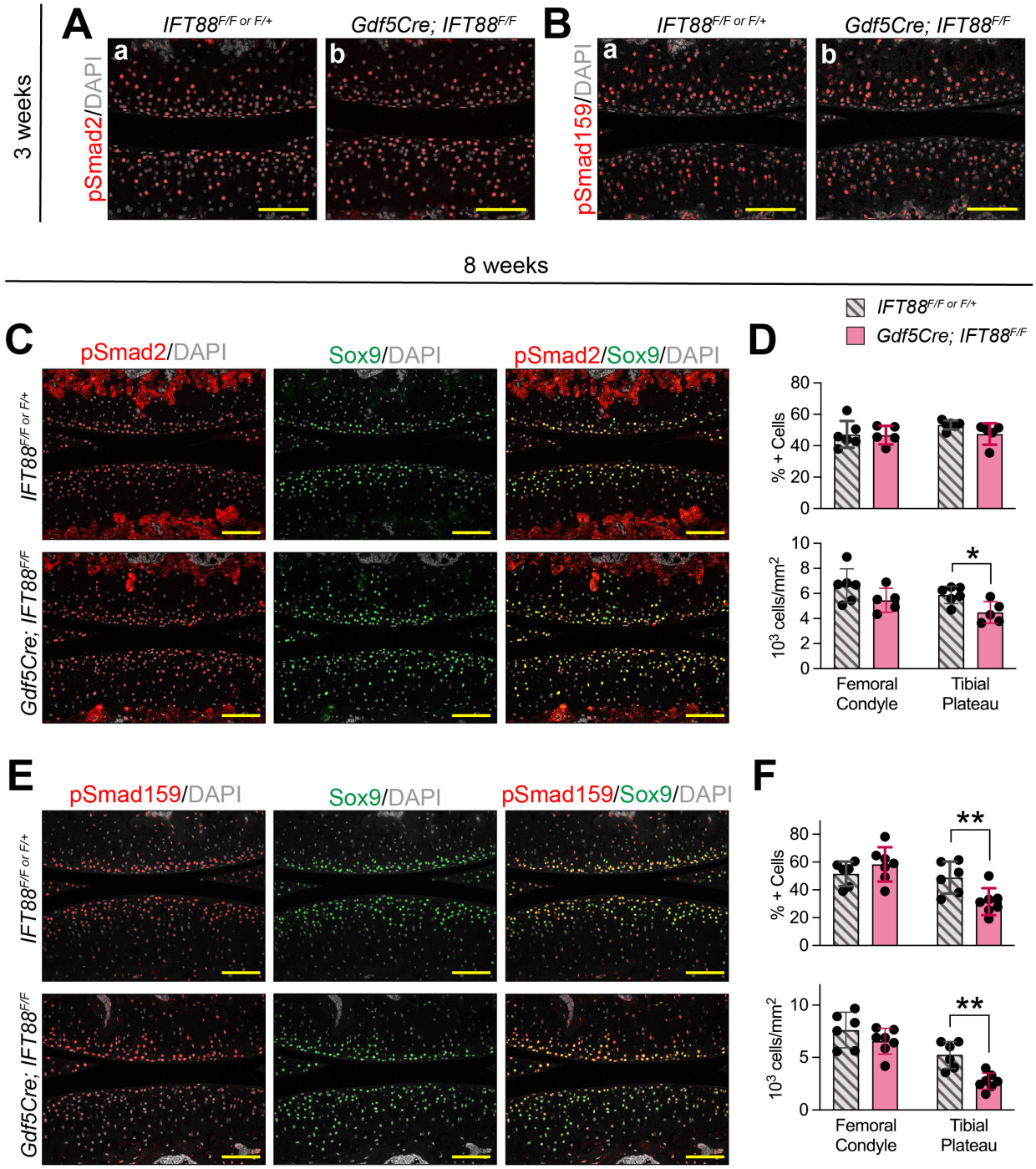

Figure 6. Loss of IFT88 alters TGFβ and BMP signaling dependent on anatomic location. (**A**) pSmad2 (TGFβ)-positive chondrocytes at 3 weeks are distributed throughout AC in both controls (a) and mutants (b). (**B**) pSmad159 (BMP)-positive chondrocytes at 3 weeks are localized in middle and bottom layers of AC in both controls (a) and mutants (b). (**C**) pSmad2 at

969 8 weeks overlaps significantly with Sox9 in both controls and mutants. (**D**) Quantification of
970 non-mineralized AC shows no change in % pSmad2-positive chondrocytes in either femoral
971 condyle or tibial plateau (top), but decreased pSmad2 chondrocyte density in the tibial plateau of
972 mutant AC (bottom). (**E**) pSmad159 at 8 weeks overlaps significantly with Sox9 in control AC
973 and femoral condyle of mutant AC, but not in the tibial plateau. (**F**) Quantification of non-
974 mineralized AC shows a significant decrease in % pSmad159-positive chondrocytes of tibial
975 plateau AC in mutants (top) and also in pSmad159 cell density in the same location (bottom).
976 scale bar = 100 μm.

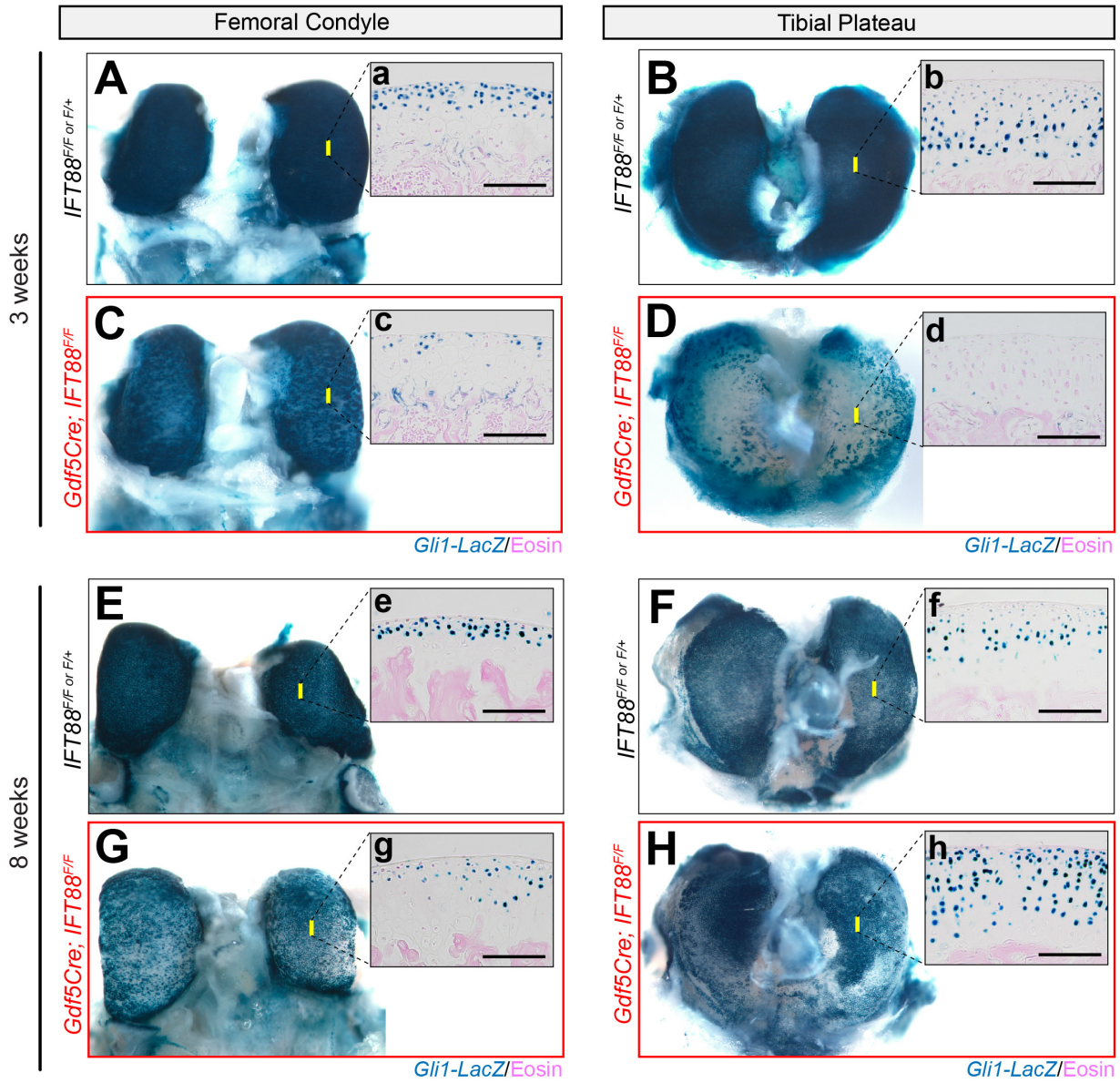

977

978 **Figure 7. Primary cilia impart age- and location-dependent functions for Hedgehog**

979 **signaling.** *Gli1-LacZ* (active hedgehog signaling) was developed by whole mount β-gal staining.

980 Yellow bars on whole mount images indicate the approximate location of tissue section images.

981 (**A-D**) *Gli1-LacZ* at 3 weeks shows many positive cells in control AC of the femoral condyle (A)

982 and tibial plateau (B). Tissue sections reveal that *Gli1-LacZ*-expressing cells localized near the

983 surface in the femoral condyle AC (a) and near the subchondral bone in the tibial plateau AC (b).

984 *Gli1-LacZ-expressing* chondrocytes are significantly decreased in mutant AC (c-d). Tissue

985 sections display patchy *Gli1-LacZ* positivity in the femoral condyle (c) and virtually no
986 expression in the tibial plateau (d). (**E-H**) *Gli1-LacZ* at 8 weeks shows many positive cells in
987 control AC of the femoral condyle (E) and tibial plateau (F). Tissue sections display similar
988 patterning established in 3 week AC (e-f). *Gli1-lacZ-expressing* cells are still significantly
989 reduced in mutant femoral condyle AC (G) but with maintained patchy expression from 3 weeks
990 (g). In mutant tibial plateau AC, *Gli1-LacZ* is generally reduced in outer regions covered by
991 meniscus and highly increased in the load-bearing center regions (H). Tissue sections from the
992 load-bearing region reveal significantly increased *Gli1-LacZ* in all layers of cells (h). Scale bar =
993 100 μm.
994

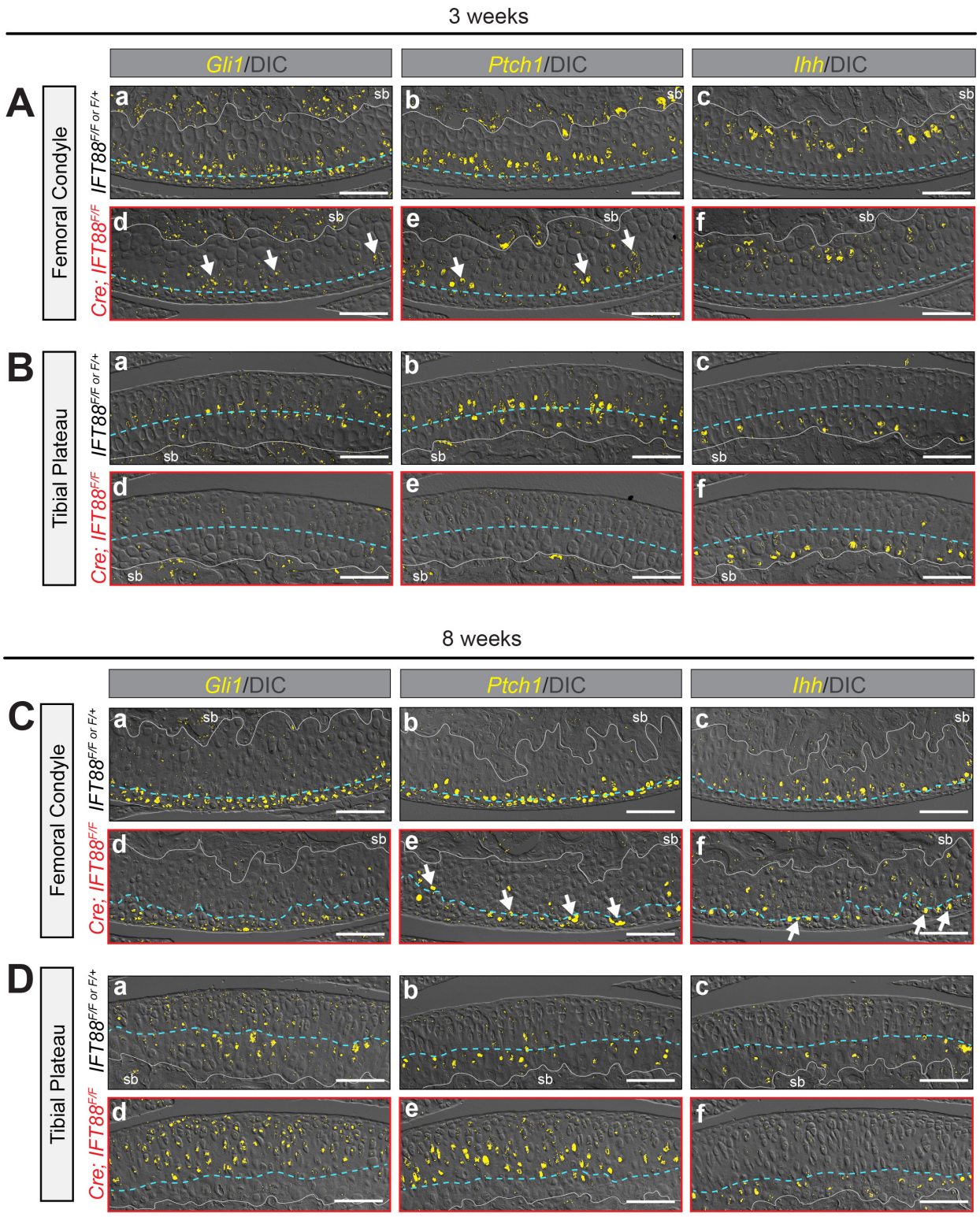

Figure 8. Hedgehog response patterning is coupled to tidemark patterning; both are disrupted in *IFT88* mutants. RNAscope detected by FastRed is visualized by confocal

998 microscopy and overlaid with DIC imaging to visualize cell morphology and tidemark
999 patterning. The blue dashed line in **A-B** represents the approximate level of the future tidemark
1000 in control AC and in **C-D** it follows the tidemark visualized by DIC. (**A**) Femoral condyle AC at
1001 3 weeks. Control AC expresses *Gli1* in multiple cell layers near the AC surface (a), *Ptch1* in 1-2
1002 cell layers around the presumptive tidemark (b) and *Ihh* in chondrocytes adjacent to the
1003 subchondral bone (c). Mutant AC displays decreased but patchy *Gli1* (d, arrows) and *Ptch1* (e,
1004 arrows) expression and normal *Ihh* in chondrocytes adjacent to the subchondral bone (f). (**B**)
1005 Tibial plateau AC at 3 weeks. Control AC expresses *Gli1* (a) and *Ptch1* (b) in similar layers
1006 surrounding the presumptive tidemark and *Ihh* in chondrocytes adjacent to the subchondral bone
1007 (c). Mutant AC displays decreased *Gli1* (d) and *Ptch1* (e) expression and normal *Ihh* in
1008 chondrocytes adjacent to the subchondral bone (f). (**C**) Femoral condyle AC at 8 weeks. Control
1009 AC expresses *Gli1* in multiple cell layers near the AC surface (a), *Ptch1* in 1-2 cell layers around
1010 the tidemark (b) and *Ihh* in chondrocytes just beneath the tidemark (c). Mutant AC displays
1011 decreased expression of *Gli1* (d), decreased and patchy expression of *Ptch1* that follows the
1012 irregular tidemark (e, arrows) and ectopic *Ihh* in non-mineralized chondrocytes (f, arrows). (**D**)
1013 Tibial plateau AC at 8 weeks. Control AC expresses *Gli1* (a) and *Ptch1* (b) in similar layers
1014 surrounding the tidemark and *Ihh* in chondrocytes just beneath the tidemark (c). Mutant AC
1015 displays increased and expanded expression of *Gli1* (d) and *Ptch1* (e) but normal *Ihh* just
1016 beneath the tidemark (f). scale bar = 100 μm.

1017 **SUPPLEMENTAL FIGURES**

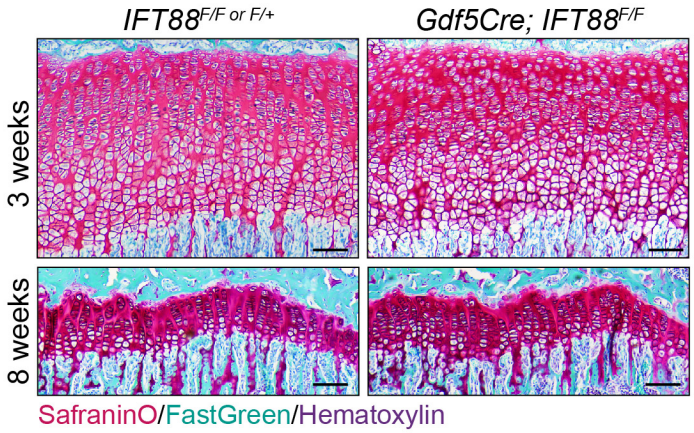

1018

1019 **Figure S1. *Gdf5Cre/+; IFT88$^{F/F}$* mutants show no alterations in growth plate patterning**

1020 **during postnatal development.** Safranin O at 3 weeks and 8 weeks shows no change in growth

1021 plate morphology in joint-specific *IFT88* conditional mutants. scale bar = 100 µm.

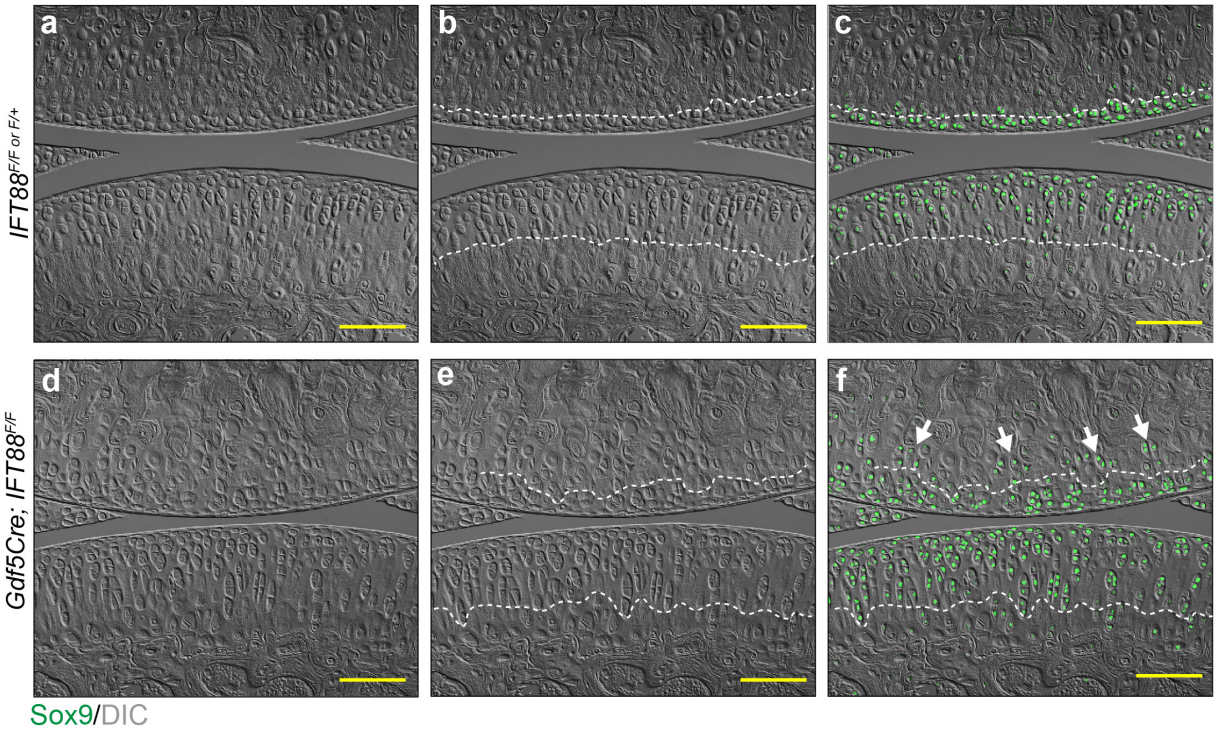

1022

1023 **Figure S2. Sox9 overlaid with DIC-imaging to visualize the tidemark in controls and**

1024 **mutants.** Sox9-stained images from Figure 3Dc-d. DIC imaging is shown without (a and d) and

1025 with (b and e) a white dashed line to denote the tidemark in controls and mutants and is overlaid

1026 with Sox9 (c and f) to show ectopic Sox9-positive chondrocytes in mutant femoral condyle AC

1027 (f, arrows). scale bar = 100 µm.

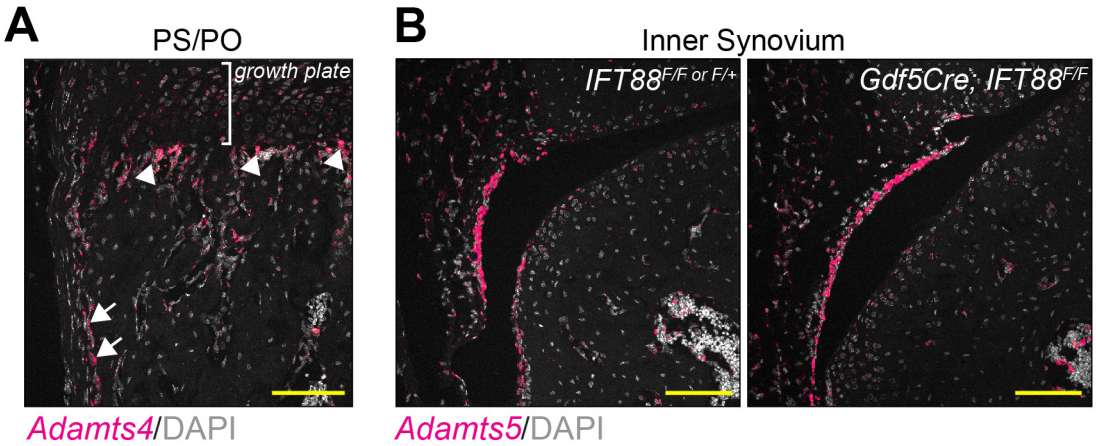

1028

1029 **Figure S3. Expression of *Adamts4* and *Adamts5* outside of AC.** RNAscope on 8 week

1030 joint/skeletal tissues developed with FastRed and imaged using confocal microscopy. (**A**)

1031 *Adamts4* is expressed the primary spongiosa beneath the growth plate (PS, arrowheads) and in

1032 the periosteum (PO, arrows). (**B**) *Adamts5* is expressed in the inner synovium of control and

1033 mutant joints. scale bar = 100 µm.

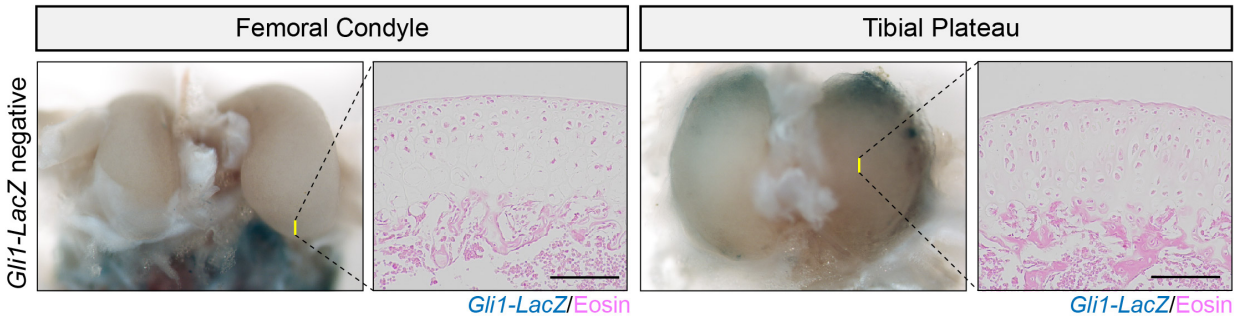

1034

1035 **Figure S4. *Gli1-LacZ* negative tissues stained with β-gal.** 3 week control, *Gli1-LacZ* negative

1036 AC stained with *Gli1-LacZ* positive AC from Figure 7. scale bar = 100 µm.